UCLA
UCLA Previously Published Works

Title
Distinct parafacial regions in control of breathing in adult rats

Permalink
https://escholarship.org/uc/item/24t6794n

Journal
PLOS ONE, 13(8)

ISSN
1932-6203

Authors
Huckstepp, Robert TR
Cardoza, Kathryn P
Henderson, Lauren E
et al.

Publication Date
2018

DOI
10.1371/journal.pone.0201485

Peer reviewed

eScholarship.org Powered by the California Digital Library
University of California

RESEARCH ARTICLE

Distinct parafacial regions in control of breathing in adult rats

Robert T. R. Huckstepp¤, Kathryn P. Cardoza, Lauren E. Henderson, Jack L. Feldman*

Department of Neurobiology, David Geffen School of Medicine, University of California Los Angeles, Los Angeles, California, United States of America

¤ Current address: School of Life Sciences, University of Warwick, Coventry, United Kingdom.
* feldman@g.ucla.edu

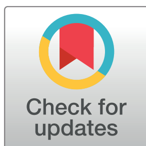

OPEN ACCESS

Citation: Huckstepp RTR, Cardoza KP, Henderson LE, Feldman JL (2018) Distinct parafacial regions in control of breathing in adult rats. PLoS ONE 13 (8): e0201485. https://doi.org/10.1371/journal.pone.0201485

Editor: Yu Ru Kou, National Yang-Ming University, TAIWAN

Received: March 1, 2018

Accepted: July 15, 2018

Published: August 10, 2018

Copyright: © 2018 Huckstepp et al. This is an open access article distributed under the terms of the Creative Commons Attribution License, which permits unrestricted use, distribution, and reproduction in any medium, provided the original author and source are credited.

Data Availability Statement: All relevant data are within the tables in the manuscript.

Funding: This work was supported by grants from the NIH, NS72211 and HL135779, awarded to JLF. The funders had no role in study design, data collection and analysis, decision to publish, or preparation of the manuscript.

Competing interests: The authors have declared that no competing interests exist.

Abstract

Recently, based on functional differences, we subdivided neurons juxtaposed to the facial nucleus into two distinct populations, the parafacial ventral and lateral regions, i.e., pF_V and pF_L. Little is known about the composition of these regions, i.e., are they homogenous or heterogeneous populations? Here, we manipulated their excitability in spontaneously breathing vagotomized urethane anesthetized adult rats to further characterize their role in breathing. In the pF_L, disinhibition or excitation decreased breathing frequency (*f*) with a concomitant increase of tidal volume (V_T), and induced active expiration; in contrast, reducing excitation had no effect. This result is congruent with pF_L neurons constituting a conditional expiratory oscillator comprised of a functionally homogeneous set of excitatory neurons that are tonically suppressed at rest. In the pF_V, disinhibition increased *f* with a presumptive reflexive decrease in V_T; excitation increased *f*, V_T and sigh rate; reducing excitation decreased V_T with a presumptive reflexive increase in *f*. Therefore, the pF_V, has multiple functional roles that require further parcellation. Interestingly, while hyperpolarization of the pF_V reduces ongoing expiratory activity, no perturbation of pF_V excitability induced active expiration. Thus, while the pF_V can affect ongoing expiratory activity, presumably generated by the pF_L, it does not appear capable of directly inducing active expiration. We conclude that the pF_L contains neurons that can initiate, modulate, and sustain active expiration, whereas the pF_V contains subpopulations of neurons that differentially affect various aspects of breathing pattern, including but not limited to modulation of ongoing expiratory activity.

Introduction

Several brainstem motor nuclei are surrounded by respiratory-related neurons [1, 2]. In the case of the facial nucleus, parafacial neurons are essential components of the breathing central pattern generator (bCPG). In particular, parafacial neurons that express the neurokinin-1 receptor (NK1R), the homeobox gene Phox2b, and the glutamate transporter VGlut2, are essential to CO_2 chemoreception [3–6]; notably, a subpopulation of these neurons have rhythmic respiratory-related activity, both *in vitro* and *in vivo* [7–9], leading us to postulate that

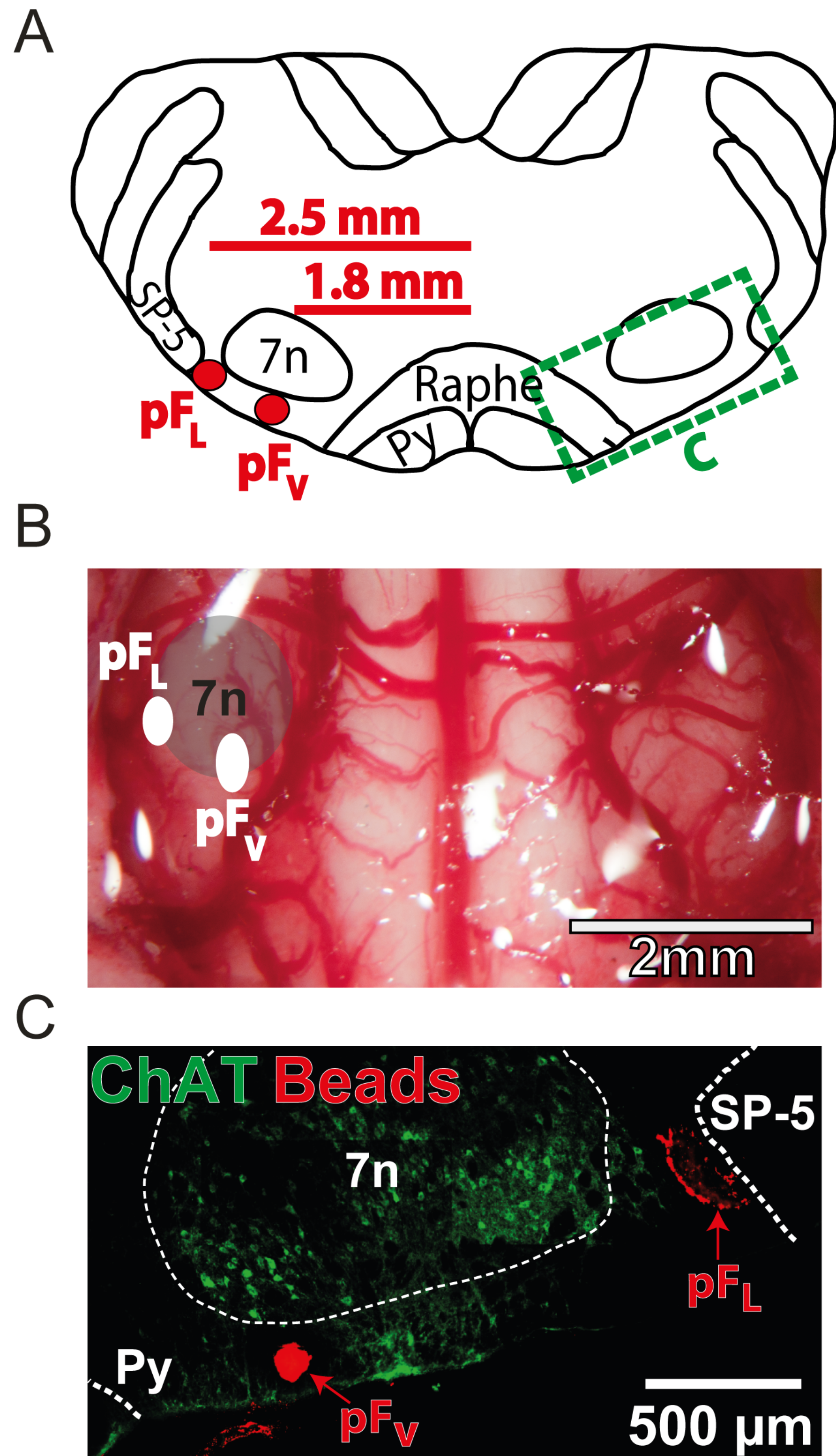

Fig 1. Histological analysis of parafacial regions. A) Localization of injections into pF_V and pF_L. Transverse view of medulla at Bregma -11.25 mm. Red circles show locations of injection sites for pF_V and pF_L. Green dashed box is magnified in C. B) Ventral view of medullary surface with location of pF_V and pF_L injection sites, marked by white circles, superimposed. C) Micrographs of injection sites. Green marks staining for choline acetyl transferase (ChAT), highlighting the cholinergic neurons of the facial (VII) nucleus, and red marks fluorescent beads coinjected with micropipette solutions in to the pF_V and pF_L. Py–Pyramidal tract, SP-5 –Spinal trigeminal tract, 7n –Facial nucleus.

https://doi.org/10.1371/journal.pone.0201485.g001

Table 1. Statistical analysis.

PARAMETER	DATA STRUCTURE	TYPE OF TEST	EFFECT SIZE	POWER	REQUIRED SAMPLE SIZE
f	Non-parametric	2-sided Wilcoxon signed-rank test	1.5	0.94	n = 8
T_I	Non-parametric	2-sided Wilcoxon signed-rank test	1.7	0.95	n = 7
T_E	Non-parametric	2-sided Wilcoxon signed-rank test	1.8	0.92	n = 6
V_T	Non-parametric	2-sided Wilcoxon signed-rank test	1.4	0.94	n = 8
Dia_{EMG}	Non-parametric	2-sided Wilcoxon signed-rank test	1.4	0.94	n = 8
GG_{EMG}	Non-parametric	2-sided Wilcoxon signed-rank test	1.7	0.95	n = 7
Abd_{EMG}	Non-parametric	2-sided Wilcoxon signed-rank test	18.5	1.0	n = 3

https://doi.org/10.1371/journal.pone.0201485.t001

breathing is driven by a dual oscillator system [10]. We identified two neighboring parafacial regions, lateral (pF_L) and ventral (pF_V) that appear to be functionally distinct components of the bCPG [11]. We hypothesized that the pF_L is a conditional expiratory oscillator that is inhibited at rest [8, 11, 12], whereas the pF_V provides a generic source of excitatory drive for both inspiration and expiration whose activity depends, at least in part, on CO_2-related signals [11, 13–15]. Furthermore, two parafacial subpopulations, containing Gastrin-Releasing Peptide and Neuromedin B (GRP and NMB, respectively) modulate sighing [16]. Therefore, further subdivision of the parafacial region into functionally distinct nuclei may be warranted, as is the case for other subcortical brain regions, such as the nucleus tractus solitarius, periaqueductal gray, and paraventricular nucleus [17–19]. To further investigate the functional contributions of the pF_L and pF_V, we selectively modulated their excitability and measured the effects on ventilation in spontaneously breathing vagotomized urethane anesthetized adult rats.

We conclude that the: i) pF_L contains a functionally homogenous population of excitatory neurons that are tonically inhibited at rest, which following an increase in excitability can initiate and maintain active expiration; ii) pF_V contains at least four functionally distinct subpopulations of neurons: three subpopulations that are tonically inhibited at rest, which can separately affect f, modulate active expiration, and modulate basal sigh rate, and one tonically active subpopulation that predominately affects V_T. Interestingly no subpopulation of pF_V neurons appears capable of directly inducing active expiration; instead the pF_V modulates active expiration generated elsewhere, presumably by effects in the pF_L and/or (pre)motoneuron pools.

Methods

All protocols were approved by the University of California Los Angeles Chancellor's Animal Research Committee. All experiments were performed in spontaneously breathing vagotomized urethane anesthetized adult Male Sprague-Dawley rats (350–450 g) rats.

Ventral approach

Anesthesia was induced with isofluorane and maintained with urethane (1.2–1.7 g/kg; Sigma) in sterile saline via a femoral catheter. Rats were placed supine in a stereotaxic apparatus on a heating pad to maintain body temperature at 37±0.5˚C. The trachea was cannulated. Respiratory flow was monitored via a flow head (GM Instruments), and CO_2 via a capnograph (Type 340: Harvard Apparatus) connected to the tracheal tube. Paired electromyographic (EMG) wires (Cooner Wire Co.) were inserted into genioglossal (GG), diaphragmatic (Dia), and oblique abdominal muscles (Abd). Anterior neck muscles were removed, a basiooccipital craniotomy exposed the ventral medullary surface, and the dura was resected. After bilateral

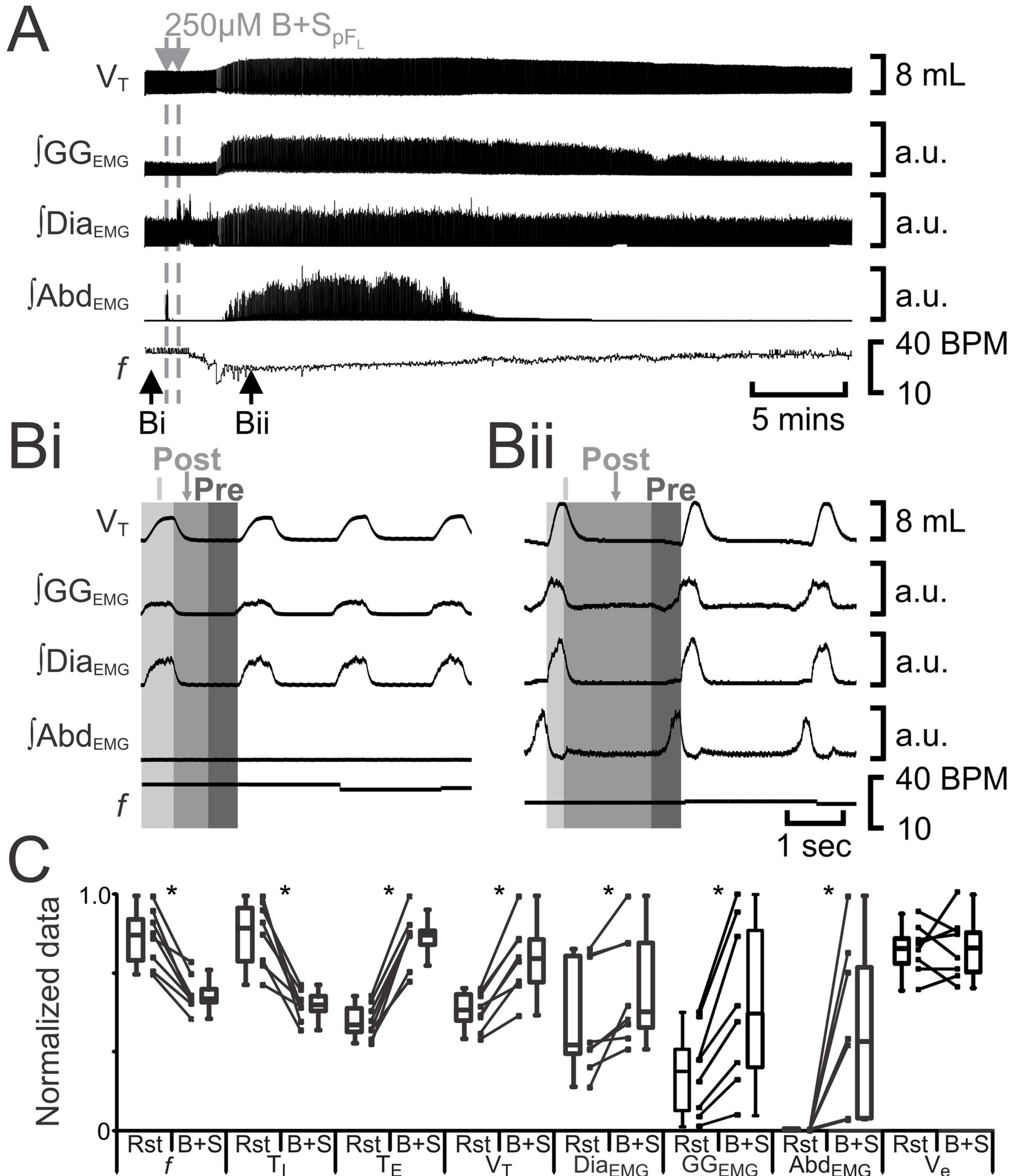
A
250μM B+S$_{pF_L}$
V_T
∫GG_{EMG}
∫Dia_{EMG}
∫Abd_{EMG}
f
8 mL
a.u.
a.u.
a.u.
40 BPM
10
5 mins
Bi
Bii
Post
Pre
1 sec
C
Normalized data
1.0
0
*
Rst
B+S
f
T_I
T_E
V_T
Dia_{EMG}
GG_{EMG}
Abd_{EMG}
V_e

Fig 2. B+S_{pFL} induces active expiration. A) Integrated traces from a single experiment. Black arrows at bottom indicate epochs in expanded traces (Bi and Bii), gray arrows at top indicate unilateral injections for B+S_{pFL}. Bi) Rest. Bii) Following B+S_{pFL}. Grey vertical boxes demark period of each breath taken up by inspiration (I; light gray), post-inspiration (Post: medium grey), and pre-inspiration (Pre: Dark gray). C) Comparison between ventilation at rest (Rst) and after B+S_{pFL} injection. Lines connect data from individual experiments, box and whisker plots show combined data. Data are normalized to highest value for each parameter, i.e., *f*, T_I, T_E, V_T, GG_{EMG}, Dia_{EMG}, or Abd_{EMG} regardless of whether it belonged to control or B+S_{pFL} group. *: $p < 0.05$. frequency–*f*, T_I–inspiratory period T_E,–expiratory period, tidal volume–V_T, GG_{EMG}–genioglossus electromyogram, Dia_{EMG}–diaphragm electromyogram, Abd_{EMG}–abdominal electromyogram. BPM–breaths per minute, a.u.—arbitrary units.

https://doi.org/10.1371/journal.pone.0201485.g002

vagotomy, exposed tissue around the neck and mylohyoid muscle were covered with dental putty (Reprosil; Dentsply Caulk) to prevent drying. Rats were left for 30 minutes for breathing to stabilize. At rest, ventilation consisted of alternating active inspiration and passive expiration. Once stabilized, solutions of drugs in micropipettes were pressure injected (100–200 nL) bilaterally using a Picospritzer II (General Valve Corp.) controlled by a Master 8 pulse generator (AMPI) into the pF_L or pF_V (Fig 1). To reduce disruption of the tissue, solutions were injected at ~50 nL/min. To ensure parity of injections of different drugs, i.e., AMPA, B+S, A +N, and consistency between both sites, i.e., pF_L and pF_V, the bilateral injections of a drug were performed ~2 mins apart. The timing between; the 2 injections of AMPA (119 ± 16 sec), the 2 injections of B+S (121 ± 10 secs), and the 2 injections of A+N (121 ± 15 secs) were not statistically different ($F_{[2, 47]} = 0.01$; p = 0.98; 2-way ANOVA), and no differences were found between the timings of the 2 injections in the pF_V (121 ± 8 secs) and the 2 injections in the pF_L (120 ± 13 secs; $F_{[1,47]} = 0.0004$; p = 0.98; 2-way ANOVA). The timing between the 2 injections of Glu before (122 ± 13 secs) and after (120 ± 13 secs) vagotomy, were also not statistically different (p = 0.8; paired T-test). After each injection rats were allowed 30–45 minutes for drugs to take effect and washout, and for baseline recordings to stabilize before the next injection.

The pF_L is defined as the area ventral to the lateral edge of the facial nucleus, juxtaposed to the spinal trigeminal tract [11]. The pF_V is defined as the area ventral to the caudal half of the facial nucleus, at a central location between the pyramidal tract and the spinal trigeminal tract [11]. Coordinates: lateral from the basilar artery, rostral from the rostral hypoglossal nerve rootlet, and dorsal from the ventral surface (in mm); pF_V: 1.8, 0.6, 0.1, and pF_L: 2.5, 0.9, 0.2.

Injections contained: i) bicuculline methylbromide (250 μM; Tocris) and strychnine hydrochloride (250 μM; Sigma) (B+S) to antagonize $GABA_A$ and glycine receptors, respectively. Injections of B+S led to disinhibition of the pF_L (B+S_{pFL}) or pF_V (B+S_{pFV}); ii) AMPA (20 μM; Sigma) to activate glutamatergic AMPA receptors. Injections of AMPA lead to excitation of the pF_L ($AMPA_{pFL}$) or pF_V ($AMPA_{pFV}$) or; iii) 2-amino-5-phosphopentanoic acid (AP-5; 1mM; Sigma) and 2,3-dihydroxy-6-nitro-7-sulfamoyl-benzo[f]quinoxaline-2,3-dione (NBQX; 1mM; Sigma) (A+N) to antagonize glutamatergic NMDA and AMPA receptors, respectively. Injections of A+N reduced excitation in the pF_L (A+N_{pFL}) or pF_V (A+N_{pFV}). All drugs were diluted in sterile saline balanced with NaOH to pH 7.35.

In one set of experiments, a ventral approach to the medulla was performed in vagus-intact rats. After a resting period to allow breathing to stabilize, rats received 100–200 nL bilateral injections of glutamate (10 mM; Sigma) administered at ~50 nL/min into the pF_V (Glu_{pFV}), following which breathing was allowed to recover. After breathing returned to baseline levels, rats were bilaterally vagotomized at the mid-cervical level. Breathing was allowed to stabilize (~30–60 mins), following which rats received a second bilateral injection of Glu_{pFV}.

Care was taken to reduce any transient effects of mechanical stimulation when placing the pipette into the tissue. As experimental controls to determine whether insertion of the pipette and injection of solution *per se* had effects, we tested the effects of saline injections.

All injections contained fluorescent beads (red fluoSpheres; Invitrogen) to allow for post-hoc identification of injection sites.

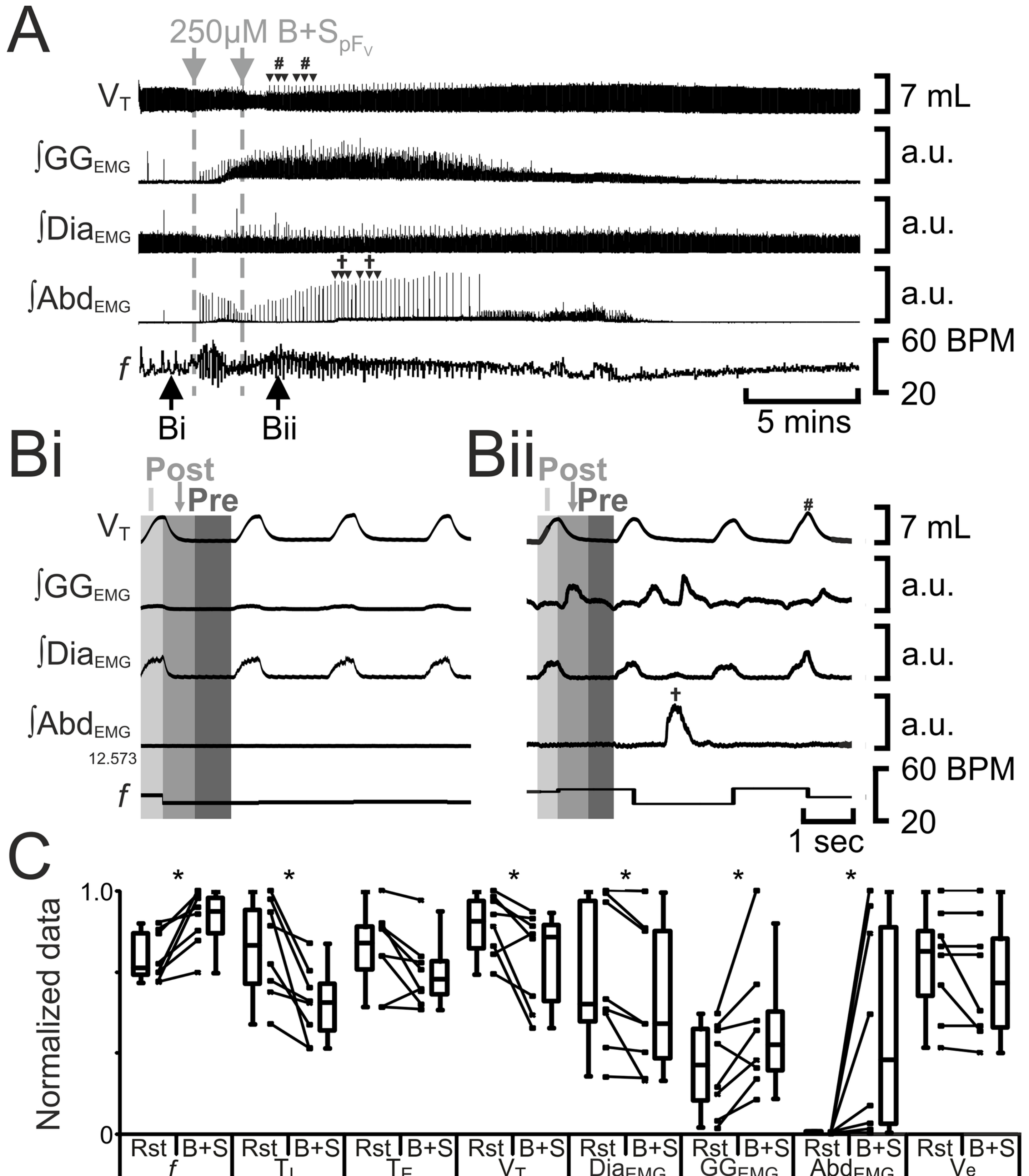

Fig 3. B+S$_{pFV}$ increases *f*, decreases V_T, and induces post-inspiratory activity in abdominal muscles and pre- and post-inspiratory activity in gengioglossus muscles. A) Integrated traces from a single experiment. Black arrows at bottom indicate epochs in expanded traces (Bi and Bii), gray arrows at top indicate unilateral

injections for $B+S_{pFV}$. Examples of sighs are marked with arrowheads labelled with #. Post-inspiratory burst Abd_{EMG}s are marked with arrowheads labelled with †. Bi) Rest. Bii) Following $B+S_{pFV}$. Grey vertical boxes demark phases of each breath: inspiration (I; light gray), post-inspiration (Post: medium grey), and pre-inspiration (Pre: Dark gray). Sigh marked by #. Post-Inspiratory Abd_{EMG} marked by †. C) Comparison between ventilation at rest (Rst) and after $B+S_{pFV}$ injection. Lines connect data from individual experiments, box and whisker plots show combined data. Data are normalized to highest value for each parameter, i.e., f, T_I, T_E, V_T, GG_{EMG}, Dia_{EMG}, or Abd_{EMG} regardless of whether it belonged to control or $B+S_{pFL}$ group. *: $p < 0.05$. Abbreviations defined in Fig 2.

https://doi.org/10.1371/journal.pone.0201485.g003

Localization of injection sites (Fig 1)

Rats were sacrificed by overdose of urethane and transcardially perfused with saline followed by cold (4˚C) paraformaldehyde (PFA; 4%). The medulla was harvested and postfixed in 4% PFA overnight at 4˚C, then cryoprotected in sucrose (30%) in standard PBS (1–3 days at 4˚C). PBS contained (mM): NaCl 137, KCl 2.7, Na_2HPO_4 10, KH_2PO_4 1.8, pH 7.4. Brainstems were transversely sectioned at 40 μm. Free-floating sections were incubated overnight in PBS containing 0.1% Triton X-100 (PBT) and mouse anti-NeuN primary antibody (1:500; EMD Millipore) or goat anti-cholineacetyl transferase (ChAT; 1:100; EMD Millipore). The tissue was washed in PBS, 6 times for 5 minutes per wash, and then incubated separately for 2–4 hours in a solution of PBT containing either donkey anti-mouse Alexa Fluor 647 secondary antibody (1:250; Jackson ImmunoResearch Laboratories, Inc.) or donkey anti-goat Alexa Fluor 488 (1:250; Invitrogen), for NeuN and ChAT, respectively. The tissue was washed in PBS, 6 times for 5 minutes. Slices were mounted onto polylysine-coated slides, dehydrated overnight at 22˚C, and coverslipped using Cytoseal 60 (Electron Microscopy Sciences). Slides were analyzed using a fluorescent microscope with AxioVision acquisition software (AxioCam2, Zeiss).

Data analysis and statistics

EMG signals and airflow measurements were collected using preamplifiers (P5; Grass Instruments) connected to a Powerlab AD board (ADInstruments) in a computer running LabChart software (ADInstruments), and were sampled at 400 Hz/channel. High pass filtered (>0.1 Hz) flow head measurements were used to calculate: tidal volume (V_T, peak amplitude of the integrated airflow signal during inspiration; pressure sensors were calibrated with a 3 mL syringe); V_T is expressed as mL. Inspiratory duration (T_I, beginning of inspiration until peak V_T), expiratory duration (T_E, peak V_T to the beginning of the next inspiration), and f ($1/[T_I+T_E]$); T_I and T_E, are expressed in secs (s), and f is expressed as breaths per minute (BPM). Minute ventilation (V_e) was calculated as f x V_T, and is expressed as mL/min. EMG data were integrated (τ = 0.05 s; $\int Dia_{EMG}$, $\int GG_{EMG}$, and $\int Abd_{EMG}$ in arbitrary units (a.u.)) and the peak amplitude of each signal computed for each cycle.

To obtain control values, all parameters were averaged for 20 respiratory cycles preceding each injection. To measure drug effect, 20 cycles were averaged during a period where the injection had its greatest effect on the airflow channel. Measurements were only made of the initial response to the drug, usually within the first 5 minutes following the 2nd injection, at a similar time as the expanded traces in the figures (marked in each figure by a black arrow with a black dotted line). Care was taken to avoid measurements where reflexive changes had taken place, for example, where the drug caused an initial decrease in breathing followed by a compensatory increase in breathing as the compound wore off. In these cases, measurements were taken at the peak effect during initial decrease and not during the reflexive increase that followed. Data was analyzed offline and exported to Excel™ (Microsoft) for further analysis. All statistical tests were performed using Igor Pro™ (WaveMetrics), except 2-way ANOVAs which were performed in OriginPro™ (OriginLab).

As described above, for each rat we calculated the average of 20 cycles preceding the stimulus ($_{control}$), and the average of 20 cycles during the stimulus ($_{stimulus}$). Both groups, the $_{control}$

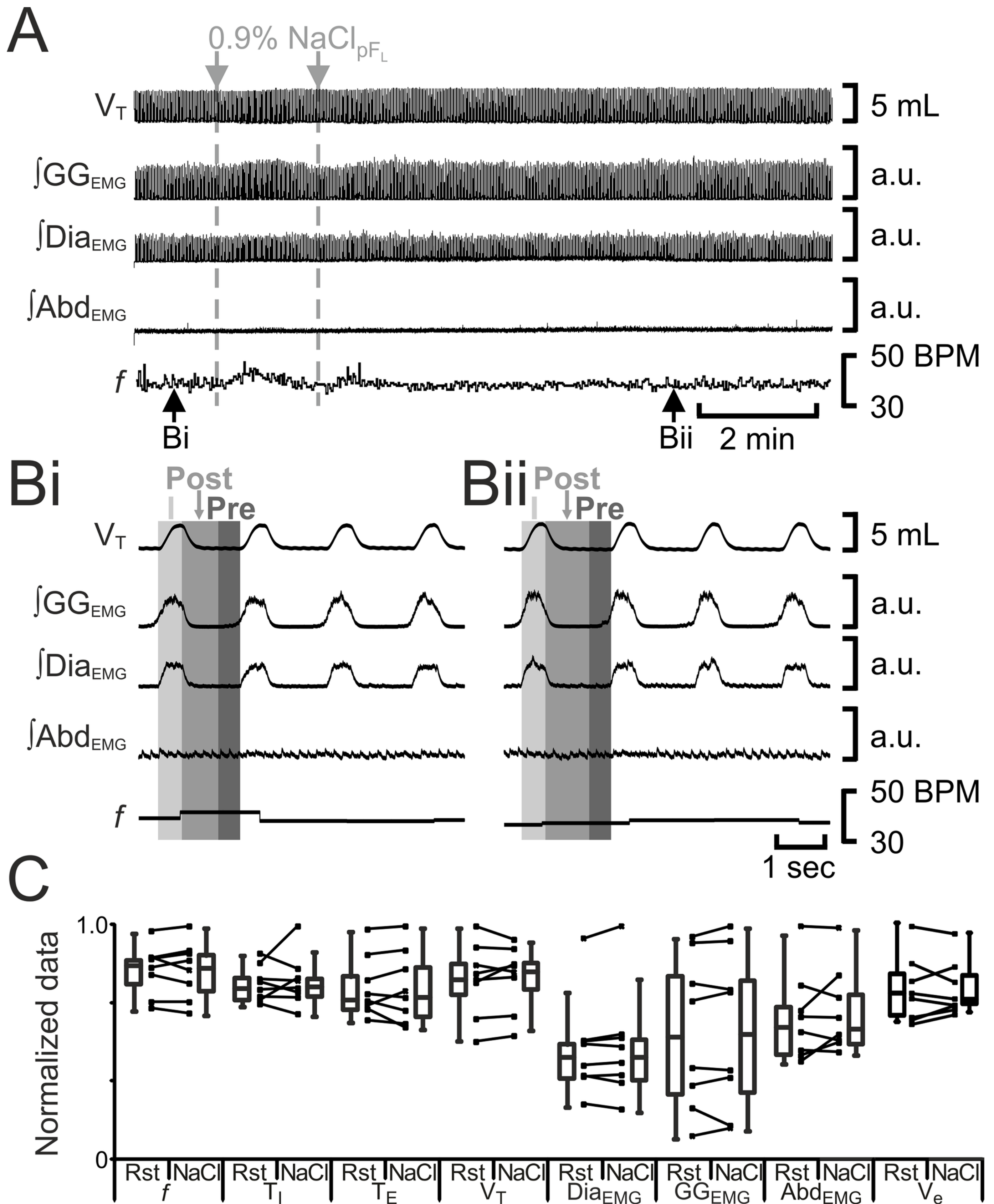
A
0.9% NaCl$_{pF_L}$
V_T
5 mL
∫GG_{EMG}
a.u.
∫Dia_{EMG}
a.u.
∫Abd_{EMG}
a.u.
f
50 BPM
30
Bi
Bii
2 min
Bi
Post
Pre
Bii
Post
Pre
1 sec
C
Normalized data
1.0
0
Rst NaCl *f*
Rst NaCl T_I
Rst NaCl T_E
Rst NaCl V_T
Rst NaCl Dia_{EMG}
Rst NaCl GG_{EMG}
Rst NaCl Abd_{EMG}
Rst NaCl V_e

Fig 4. Saline_{pFL} does not affect breathing. A) Integrated traces from a single experiment. Black arrows at bottom indicate epochs in expanded traces (Bi and Bii), gray arrows at top indicate unilateral injections for Saline_{pFL}. Bi) Rest. Bii) Following Saline_{pFL}. Grey vertical boxes demark phases of each breath: inspiration (I; light gray), post-inspiration (Post: medium grey), and pre-inspiration (Pre: Dark gray). a.u.: arbitrary units. C) Comparison between ventilation at rest (Rst) and after Saline_{pFL}. Lines connect data from individual experiments, box and whisker plots show combined data. Data are normalized to highest value for that parameter, i.e., *f*, $T_{I,}$ T_E, V_T, GG_{EMG}, Dia_{EMG}, or Abd_{EMG} regardless of whether it belonged to control or saline_{pFL} group. Abbreviations defined in Fig 2.

https://doi.org/10.1371/journal.pone.0201485.g004

values and their associated $_{\text{stimulus}}$ value for every rat, were combined into a single data set. To facilitate graphical comparisons data was normalized to the highest value in the data set regardless of whether it belonged to $_{\text{control}}$ or $_{\text{stimulus}}$ group. Therefore, the highest value in the data set, whether it be $_{\text{control}}$ or $_{\text{stimulus}}$, was 1.0.

We define active expiration as the epoch of appearance of burst activity in expiratory muscles, i.e., abdominals, that leads to forced air outflow, typically during late expiration, and consequently, increased V_T in the following inspiration. We define sighs by their characteristic augmented V_T caused by a second inspiratory effort that occurs before the initial eupneic inspiration is complete. These augmented breaths result from largely from high amplitude inspiratory Dia_{EMG}.

Data were not normally distributed. Data were therefore analyzed using the non-parametric 2-sided Wilcoxon signed-rank test with a significance level of $P \leq 0.05$ and reported as median and interquartile range (IQR). Data are displayed as box and whisker plots for comparison of groups, and as line graphs for individual experiments. There were 8 biological repeats and no technical repeats in all data sets, with 2 exceptions: Statistical outliers were excluded from the data if they failed both Pierce's criterion and Grubb's test; this led to the removal of 1 outlier from the Abd_{EMG} data from the $AMPA_{pFV}$ and $AMPA_{pFL}$ data sets.

Power analysis was calculated in G*Power3 (http://www.gpower.hhu.de/en.html [20]), using a Wilcoxon signed rank tests (matched pairs): with an α error probability of 0.05, and a power (1-β error probability) of 0.90, and effect sizes were calculated from the data (Table 1).

Results

Disinhibition of pF_L or pF_V affect breathing pattern (Figs 2–5, Table 2)

Disinhibition of pF_L neurons by the GABAergic antagonist bicuculline and the glycine antagonist strychnine ($B+S_{pFL}$) can induce active expiration [8, 11], which we confirm here. Bilateral injection of $B+S_{pFL}$ (n = 8) decreased *f* and T_I, increased T_E, V_T, $\int Dia_{EMG}$, and inspiratory-related $\int GG_{EMG}$ activity, and induced rhythmic expiratory bursting in $\int GG_{EMG}$ and $\int Abd_{EMG}$ (Fig 2), the latter a signature of active expiration, q.v., [8, 11]. Bilateral $B+S_{pFL}$ had no effect on minute ventilation (V_e) due to a compensatory increase in V_T in response to the changes in *f* elicited by the antagonism of the inhibitory receptors.

Disinhibition of pF_V neurons by unilateral injection of bicuculline increases V_T with a reciprocal decrease in *f* in awake rats [21]. Furthermore, pF_V appears to facilitate active expiration through projections to abdominal and genioglossus motoneurons, but does not itself induce active expiration [11]. We therefore expected that pF_V disinhibition with a cocktail of bicuculline and strychnine ($B+S_{pFV}$) would increase V_E, as well as alter abdominal and genioglossus activity, but would not induce active expiration. Bilateral injections of $B+S_{pFV}$ (n = 8) increased *f*, decreased T_I, did not alter T_E, and decreased V_T and $\int Dia_{EMG}$. Bilateral $B+S_{pFV}$ in anesthetized rats did not alter V_E due to a compensatory decrease in V_T in response to an increase in *f* elicited by the antagonism of inhibitory receptors, which is the opposite response to unilateral injection of bicuculine in the same region in awake rats [21]. pF_V disinhibition had multiple effects on genioglossus activity, increasing inspiratory-related $\int GG_{EMG}$ and

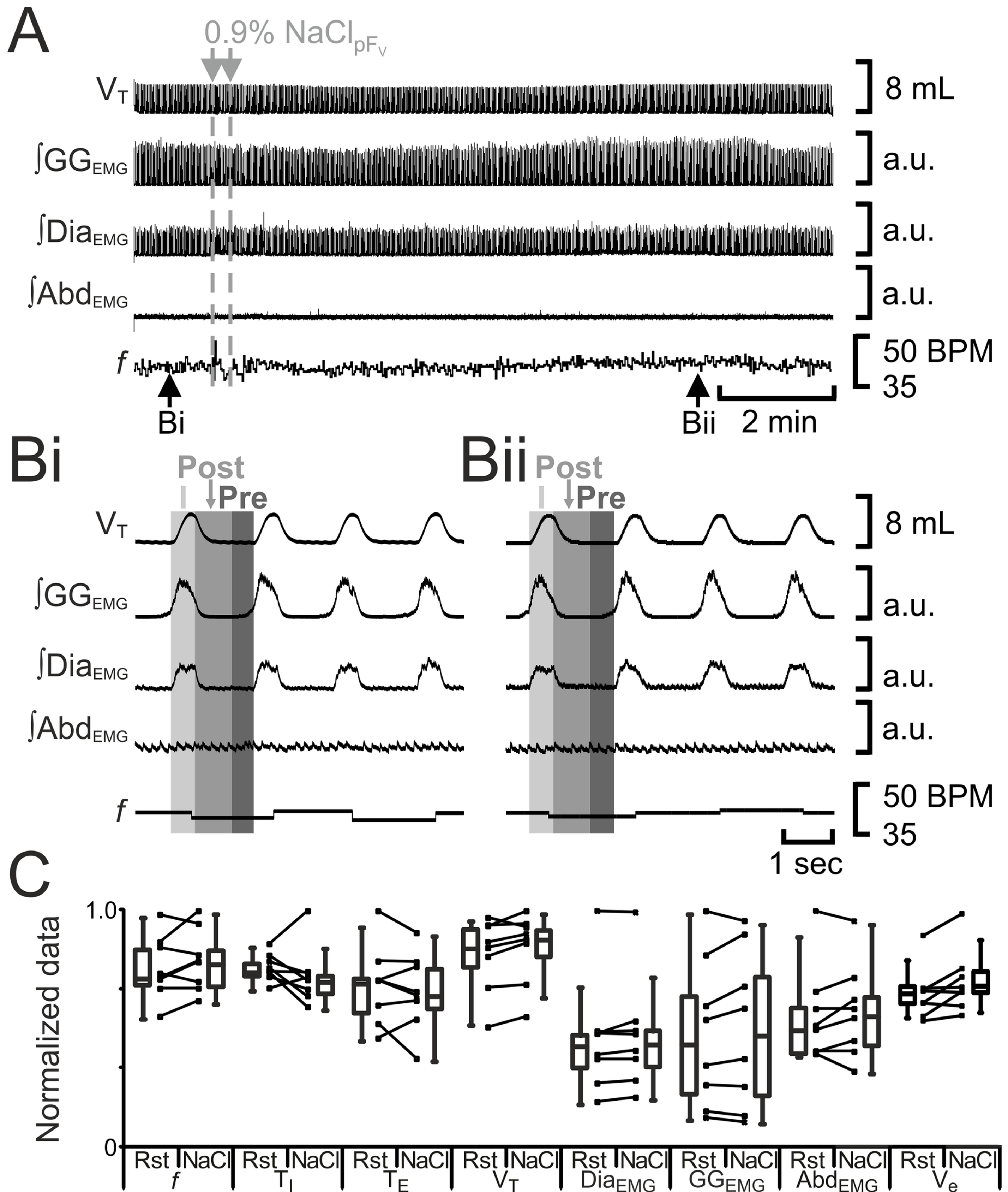
A
0.9% NaCl$_{pF_V}$
V_T
∫GG_{EMG}
∫Dia_{EMG}
∫Abd_{EMG}
f
8 mL
a.u.
a.u.
a.u.
50 BPM
35
Bi
Bii
2 min
Bi
Bii
Post
Pre
1 sec
C
Normalized data
1.0
0
Rst
NaCl
f
T_I
T_E
V_T
Dia_{EMG}
GG_{EMG}
Abd_{EMG}
V_e

Fig 5. $Saline_{pFV}$ does not affect breathing. A) Integrated traces from a single experiment. Black arrows at bottom indicate epochs in expanded traces (Bi and Bii), gray arrows at top indicate unilateral injections for $Saline_{pFV}$. Bi) Rest. Bii) Following $Saline_{pFV}$. Grey vertical boxes demark phases of each breath: inspiration (I; light gray), post-inspiration (Post: medium grey), and pre-inspiration (Pre: Dark gray). a.u.: arbitrary units. C) Comparison between ventilation at rest (Rst) and after $Saline_{pFV}$. Lines connect data from individual experiments, box and whisker plots show combined data. Data are normalized to highest value for that parameter, i.e., f, T_I, T_E, V_T, GG_{EMG}, Dia_{EMG}, or Abd_{EMG} regardless of whether it belonged to control or $Saline_{pFV}$ group. Abbreviations defined in Fig 2.

https://doi.org/10.1371/journal.pone.0201485.g005

inducing both pre-inspiratory and post-inspiratory $\int GG_{EMG}$ activity (Fig 3). In 6 out of 8 experiments, $B+S_{pFV}$ also induced high amplitude post-inspiratory Abd_{EMG} activity (Fig 3A† and 3Bii†), which while rhythmic was slow, occurring every 10 ± 1 breaths. This pattern of high amplitude post-inspiratory Abd_{EMG} activity was distinct from active expiration that

Table 2. Median and interquartile range for all recorded variables.

A) *pF*	f (BPM)	T_I (secs)	T_E (secs)	V_T (mL)	Dia_{EMG} (a.u.)	GG_{EMG} (a.u.)	Abd_{EMG} (a.u.)	V_e ($mL \cdot min^{-1}$)
Rest	44, 9	0.5, 0.1	1.0, 0.2	5.3, 1.1	26, 30	9, 9	0, 0	218, 30
B+S	28, 3	0.3, 0.0	1.8, 0.1	7.5, 1.9	36, 26	17, 20	16, 27	219, 47
P =	0.008	0.008	0.008	0.008	0.008	0.008	0.008	0.9
Rest	45, 8	0.4, 0.1	0.9, 0.3	5.2, 1.1	25, 22	6, 8	0, 0	212, 52
AMPA	32, 14	0.3, 0.1	1.5, 0.8	6.1, 1.0	29, 23	13, 10	2, 3	177, 7
P =	0.008	0.02	0.008	0.008	0.02	0.008	0.02	0.1
Rest	54, 11	0.3, 0.1	0.7, 0.2	4.2, 0.7	28, 24	6, 8	0, 0	215, 43
A+N	59, 10	0.4, 0.1	0.6, 0.2	3.9, 1.1	27, 25	6, 7	0, 0	213, 28
P =	0.4	0.4	0.3	0.8	0.5	0.2	0.4	0.9
B) pF_V								
Rest	37, 9	0.5, 0.2	1.1, 0.9	5.4, 1.2	28, 26	11, 11	0, 0	207, 22
B+S	50, 8	0.3, 0.1	0.9, 0.2	5.0, 1.9	24, 28	14, 9	7, 18	229, 80
P =	0.008	0.008	0.054	0.02	0.008	0.04	0.008	0.5
Rest	42, 6	0.5, 0.1	1.0, 0.2	5.2, 0.7	25, 29	7, 77	0, 0	210, 39
AMPA	47, 4	0.3, 0.1	0.9, 0.2	5.5, 1.2	30, 28	13, 11	0, 0	262, 40
P =	0.02	0.008	0.2	0.04	0.02	0.008	0.7	0.02
Rest	48, 8	0.43, 0.1	0.8, 0.2	4.7, 0.9	28, 24	7, 8	0, 0	217, 16
A+N	61, 22	0.36, 0.1	0.6, 0.2	3.7, 0.8	26, 23	3, 5	0, 0	205, 33
P =	0.02	0.02	0.04	0.008	0.02	0.008	0.4	0.3
C) *Glutamate*-pF_V								
VI Rest	104, 53	0.21, 0.08	0.3, 0.1	2.1, 0.7	15, 13	3, 4	0, 0	254, 34
VI Glu	87, 39	0.23, 0.09	0.4, 0.2	2.4, 0.9	16, 15	5, 5	0, 0	232, 51
P =	0.03	0.02	0.02	0.046	0.02	0.02	0.9	0.4
Vx Rest	46, 20	0.34, 0.26	0.8, 0.4	2.8, 1.9	20, 16	10, 16	0, 0	163, 31
Vx Glu	49, 19	0.26, 0.26	0.8, 0.4	3.0, 2.1	22, 23	13, 19	0, 0	196, 45
P =	0.03	0.03	0.4	0.03	0.03	0.03	0.2	0.03
D) *Saline*								
Rest	44, 9	0.3, 0.0	1.0, 0.2	3.8, 0.9	35, 10	13, 12.	0, 0	202, 23
pF_V	48, 9	0.3, 0.0	0.9, 0.2	4.0, 0.5	36, 12	14, 15	0, 0	212, 28
P =	0.3	0.3	0.5	0.8	0.1	0.4	0.5	0.08
Rest	48, 6	0.3, 0.0	0.9, 0.2	3.9, 0.7	35, 11	14, 13	0, 0	48, 6
pF_L	48, 9	0.3, 0.0	1.0, 0.3	4.1, 0.6	35, 13	15, 13	0, 0	48, 9
P =	0.9	0.9	1.0	0.5	0.7	0.5	0.7	0.6

A-B) Agonists and antagonists injected into the pF_L (A) and pF_V (B). C) Glutamate injected into the pFv of vagus-intact (VI) and vagotomized (Vx) rats. D) Saline injected into the pFv or pFL. All tables display data as: median, IQR.

https://doi.org/10.1371/journal.pone.0201485.t002

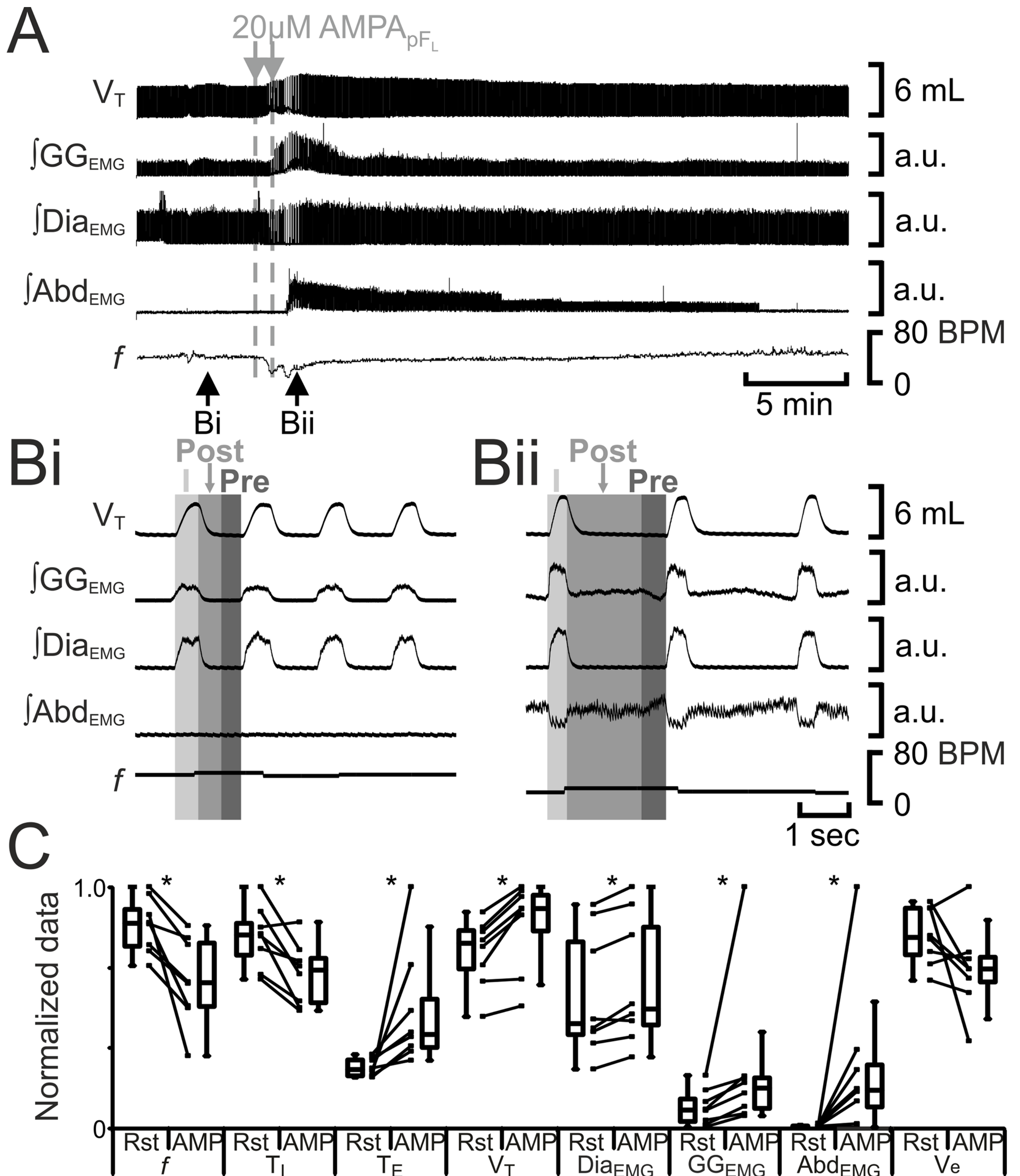
A
20μM AMPA$_{pF_L}$
V_T
∫GG_{EMG}
∫Dia_{EMG}
∫Abd_{EMG}
f
6 mL
a.u.
a.u.
a.u.
80 BPM
0
5 min
Bi
Bii
Bi
Post
Pre
Bii
Post
Pre
6 mL
a.u.
a.u.
a.u.
80 BPM
0
1 sec
C
Normalized data
1.0
0
Rst AMP f
Rst AMP T_I
Rst AMP T_E
Rst AMP V_T
Rst AMP Dia_{EMG}
Rst AMP GG_{EMG}
Rst AMP Abd_{EMG}
Rst AMP Ve

Fig 6. $AMPA_{pFL}$ induces active expiration. A) Integrated traces from a single experiment. Black arrows at bottom indicate epochs in expanded traces (Bi and Bii), gray arrows at top indicate unilateral injections for $AMPA_{pFL}$. Bi) Rest. Bii) Following $AMPA_{pFL}$. Grey vertical boxes demark phases of each breath: inspiration (I; light gray), post-inspiration (Post: medium grey), and pre-inspiration (Pre: Dark gray). C) Comparison between ventilation at rest (Rst) and after $AMPA_{pFL}$ injection. Lines connect data from individual experiments, box and whisker plots show combined data. Data are normalized to highest value for each parameter, i.e., f, T_I, T_E, V_T, GG_{EMG}, Dia_{EMG}, or Abd_{EMG} regardless of whether it belonged to control or $AMPA_{pFL}$ group. *: $p < 0.05$. Abbreviations defined in Fig 2.

https://doi.org/10.1371/journal.pone.0201485.g006

occurs between every inspiration at a lower amplitude (see Fig 2 and [8, 11]. Interestingly, coincident with high amplitude post-inspiratory Abd_{EMG} bursts, there was inhibition of GG_{EMG} activity, showing co-ordination between GG_{EMG} and ABD_{EMG} during expiration (Fig 3B). In all experiments, $B+S_{pFV}$ also induced sighs i.e., augmented breaths with high amplitude inspiratory Dia_{EMG} followed by prolonged T_E (Fig 3A# and 3Bii#); sighs were rhythmic but slow, occurring every 12 ± 1 breaths. The high amplitude post-inspiratory Abd_{EMG} activity was not coordinated with sighing.

To test for any nonspecific effects of pF_V or pF_L injections on breathing, we injected saline into both regions. In anesthetized rats, saline injections in the pF_L (n = 8) did not alter f, T_I, T_E, V_T, $\int Dia_{EMG}$, GG_{EMG}, $\int Abd_{EMG}$, or V_E (Fig 4). In anesthetized rats, saline injections in the pF_V (n = 8) did not alter f, T_I, T_E, V_T, $\int Dia_{EMG}$, $\int GG_{EMG}$, $\int Abd_{EMG}$, or V_E (Fig 5).

Excitation of either pF_L or pF_V affects breathing pattern (Figs 6–8, Table 2)

Photostimulation of pF_L neurons elicits active expiration [8]. We predicted that excitation of the pF_L with the glutamatergic agonist AMPA ($AMPA_{pFL}$) would also elicit active expiration. Bilateral injections of $AMPA_{pFL}$ (n = 8) decreased f and T_I, and increased T_E, V_T, $\int Dia_{EMG}$, inspiratory-related $\int GG_{EMG}$ activity and $\int Abd_{EMG}$ (Fig 6), the latter a signature of active expiration, q.v., [8, 11]. Like $B+S_{pFL}$, bilateral injections of $AMPA_{pFL}$ did not affect V_e, presumably due to a compensatory increase in V_T in response to the decrease in f.

Excitation of pF_V neurons by injection of glutamate increases phrenic nerve discharge amplitude and induces sighing in urethane anesthetized, paralyzed, artificially ventilated, vagotomized cats [22]; photostimulation of pF_V neurons leads to increased sighing and respiratory frequency in conscious rats [23]. We predicted that excitation of the pF_V with AMPA ($AMPA_{pFV}$) would increase ventilation and sighing. Bilateral injection of $AMPA_{pFV}$ (n = 8) increased f, decreased T_I, did not alter T_E, and increased V_T, $\int Dia_{EMG}$, and inspiratory-related $\int GG_{EMG}$, but neither induced expiratory-modulated GG_{EMG} nor Abd_{EMG} (Fig 7). Unlike $B+S_{pFV}$, bilateral injections of $AMPA_{pFV}$ increased V_E due to increases in both V_T and f. In 5 out of 8 rats, before $AMPA_{pFV}$ caused V_T to reach maximal amplitude it induced 1–2 sigh like events, but with no associated GG_{EMG} or Abd_{EMG} activity (data not shown).

The lack of induction of sighing could have been due to either the increased V_T in vagotomized rats, or due to the lack of activation of other glutamatergic receptors, e.g., NMDA, mGluR, etc, in addition to AMPA receptors. To explore these possibilities, in separate experiments, we injected glutamate into the pF_V (Glu_{pFV}) of anesthetized rats before and after vagotomy. Before vagotomy (n = 8), bilateral Glu_{pFV} decreased f, increased T_I, T_E, V_T, $\int Dia_{EMG}$, inspiratory-related $\int GG_{EMG}$ (Fig 8), and sigh rate, but neither induced expiratory-modulated GG_{EMG} nor Abd_{EMG} (Fig 8). Bilateral injections of Glu_{pFV} did not affect V_E due to a compensatory decrease in f in response to an increase in V_T, elicited by the activation of glutamate receptors. Following vagotomy, bilateral Glu_{pFV} increased f, decreased T_I, did not alter T_E, and increased V_T, $\int Dia_{EMG}$, and inspiratory-related $\int GG_{EMG}$, but neither induced expiratory-modulated GG_{EMG} nor Abd_{EMG} (Fig 8), similar to $AMPA_{pFV}$ (Fig 7). Like $AMPA_{pFV}$, bilateral injections of Glu_{pFV} increased V_E due to increases in both V_T and f. In 3 out of 6 vagotomized

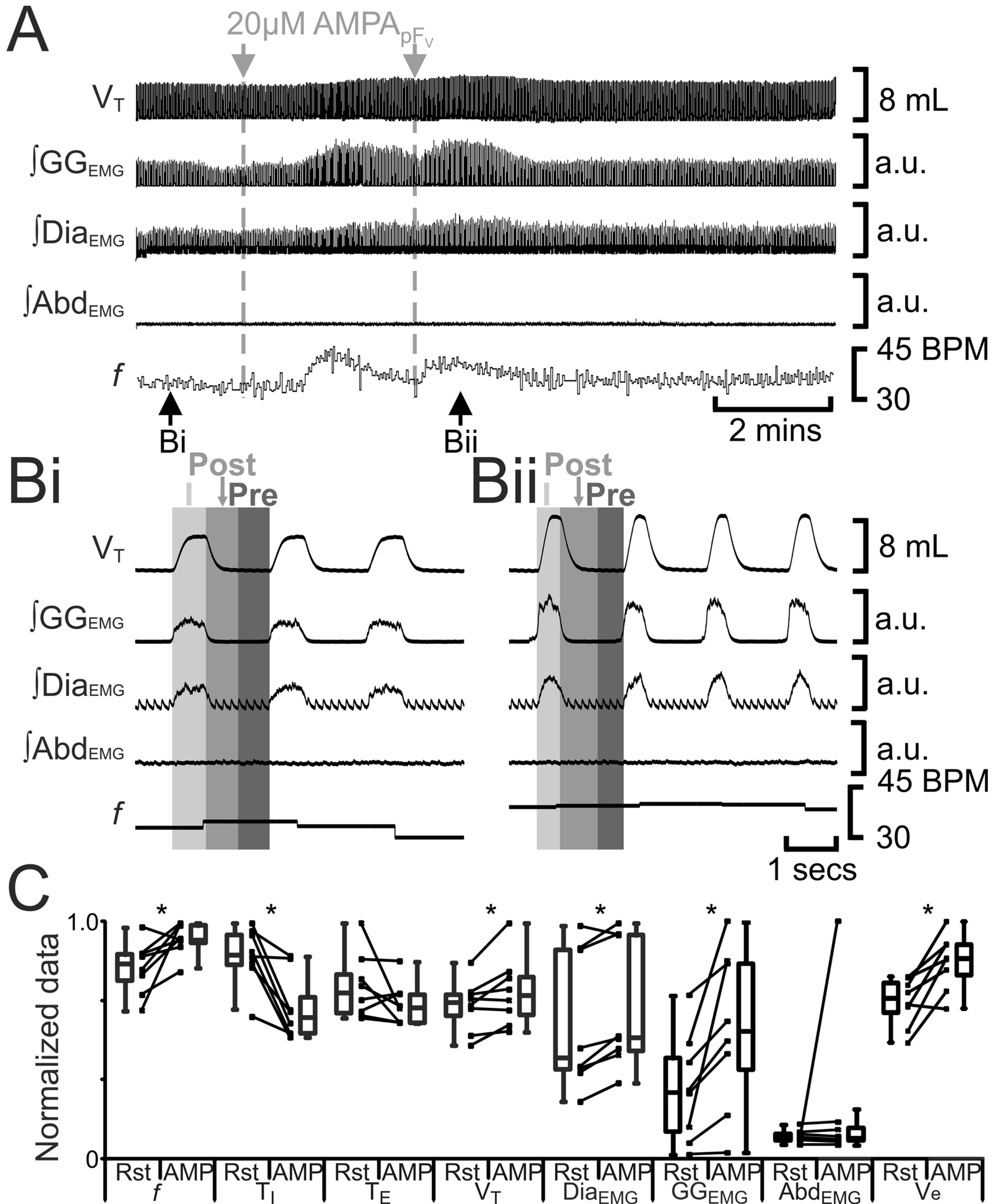
A
20μM AMPA pFV
VT
∫GGEMG
∫DiaEMG
∫AbdEMG
f
8 mL
a.u.
a.u.
a.u.
45 BPM
30
2 mins
Bi
Bii
Bi
Post
Pre
Bii
Post
Pre
VT
∫GGEMG
∫DiaEMG
∫AbdEMG
f
8 mL
a.u.
a.u.
a.u.
45 BPM
30
1 secs
C
Normalized data
1.0
0
Rst AMP f
Rst AMP TI
Rst AMP TE
Rst AMP VT
Rst AMP DiaEMG
Rst AMP GGEMG
Rst AMP AbdEMG
Rst AMP Ve
*

Fig 7. $AMPA_{pFV}$ increases *f* and V_T, but does not induce post-inspiratory activity in either abdominal muscles or in pre- and post-inspiratory activity gengioglossus muscles. A) Integrated traces from a single experiment. Black arrows at bottom indicate epochs in expanded traces (Bi and Bii), gray arrows at top indicate unilateral injections for $AMPA_{pFV}$. Bi) Rest. Bii) Following $AMPA_{pFV}$. Grey vertical boxes demark phases of each breath: inspiration (I; light gray), post-inspiration (Post: medium grey), and pre-inspiration (Pre: Dark gray). C) Comparison between ventilation at rest (Rst) and after $AMPA_{pFV}$ injection. Lines connect data from individual experiments, box and whisker plots show combined data. Data are normalized to highest value for each parameter, i.e., *f*, T_I, T_E, V_T, GG_{EMG}, Dia_{EMG}, or Abd_{EMG} regardless of whether it belonged to control or $AMPA_{pFV}$ group. *: $p < 0.05$. Abbreviations defined in Fig 2.

https://doi.org/10.1371/journal.pone.0201485.g007

rats, before Glu_{pFV} caused V_T to reach maximal amplitude it induced 3–6 sigh-like events but with no associated GG_{EMG} or Abd_{EMG} (data not shown).

Reduced excitation of pF_V and pF_L have different effects on breathing (Figs 9 and 10, Table 2)

Many, if not most or all, pF_L neurons are silent at rest [8, 24]; not surprisingly, hyperpolarizing pF_L neurons at rest does not affect ventilation [11]. We predicted that reduction of pF_L excitability with local injection of a cocktail of the glutamatergic antagonists AP-5 and NBQX ($A+N_{pFL}$) would not affect breathing. Bilateral injections of $A+N_{pFL}$ (n = 8) had no effect on *f*, T_I, T_E, V_T, $\int Dia_{EMG}$, or $\int GG_{EMG}$; Abd_{EMG} silent at rest, remained so after $A+N_{pFL}$ (Fig 9). Bilateral injections of $A+N_{pFL}$ did not affect V_E as it neither affected V_T nor *f*.

By contrast, pF_V neurons are active at rest, providing excitatory drive for quiet breathing [25–29]; hyperpolarizing pF_V neurons reduces ventilation [5, 11, 13]. We predicted that reduction of pF_V excitability with local injection of AP-5 and NBQX ($A+N_{pFV}$), would reduce ventilation. Bilateral $A+N_{pFV}$ (n = 8) increased *f*, decreased T_I and T_E, V_T, $\int Dia_{EMG}$, and $\int GG_{EMG}$; Abd_{EMG}, silent at rest, remained so after $A+N_{pFV}$ (Fig 10). Bilateral injections of $A+N_{pFV}$ did not affect V_E due to a compensatory increase in *f* in response to a decrease in V_T, elicited by the activation of glutamate receptors. That no injection into the pF_V induced active expiration is indicative that the injectate did not spread to the adjacent pF_L, likewise since $A+N_{pFL}$ did not induce any changes in breathing, this indicates the injectate did not spread to the adjacent pF_V.

Discussion

Since the putative identification of a conditional expiratory oscillator in the rostral medulla [10, 12, 30], attention has focused on regions surrounding the facial nucleus as its location [8, 11, 15, 24, 31]. We identified two functionally separate parafacial regions: the pF_V and pF_L [11]. We propose that the pF_V provides a critical generic drive to breathe, driving inspiration at rest and facilitating both inspiration and expiration when chemosensory drive increases [11, 15], and that the pF_L is silent at rest, but once activated, drives active expiration [8, 11]. Additionally, there appears to be a third parafacial region, more dorsocaudal, containing neurons expressing gastrin releasing peptide that modulates baseline sigh rate [16]. Thus, there appear to be several distinct parafacial regions contributing to the bCPG. To further investigate the role of parafacial neurons, and the neuronal composition of parafacial regions at the ventral medullary surface, we pharmacologically altered the excitability of pF_V and pF_L neurons and measured the effects on breathing.

Further support of the hypothesis of the pF_L as the source for active expiration

Antagonizing ionotropic glutamate receptors with $A+N_{pFL}$ did not alter any respiratory parameter, i.e., no change in *f*, T_I, T_E, V_T, Dia_{EMG}, GG_{EMG}, or Abd_{EMG}, supporting our previous observation that these neurons are silent at rest, q.v., [8, 11]. In the pF_L, excitation (with AMPA) or disinhibition (by antagonizing ionotropic GABA and glycine receptors with B+S)

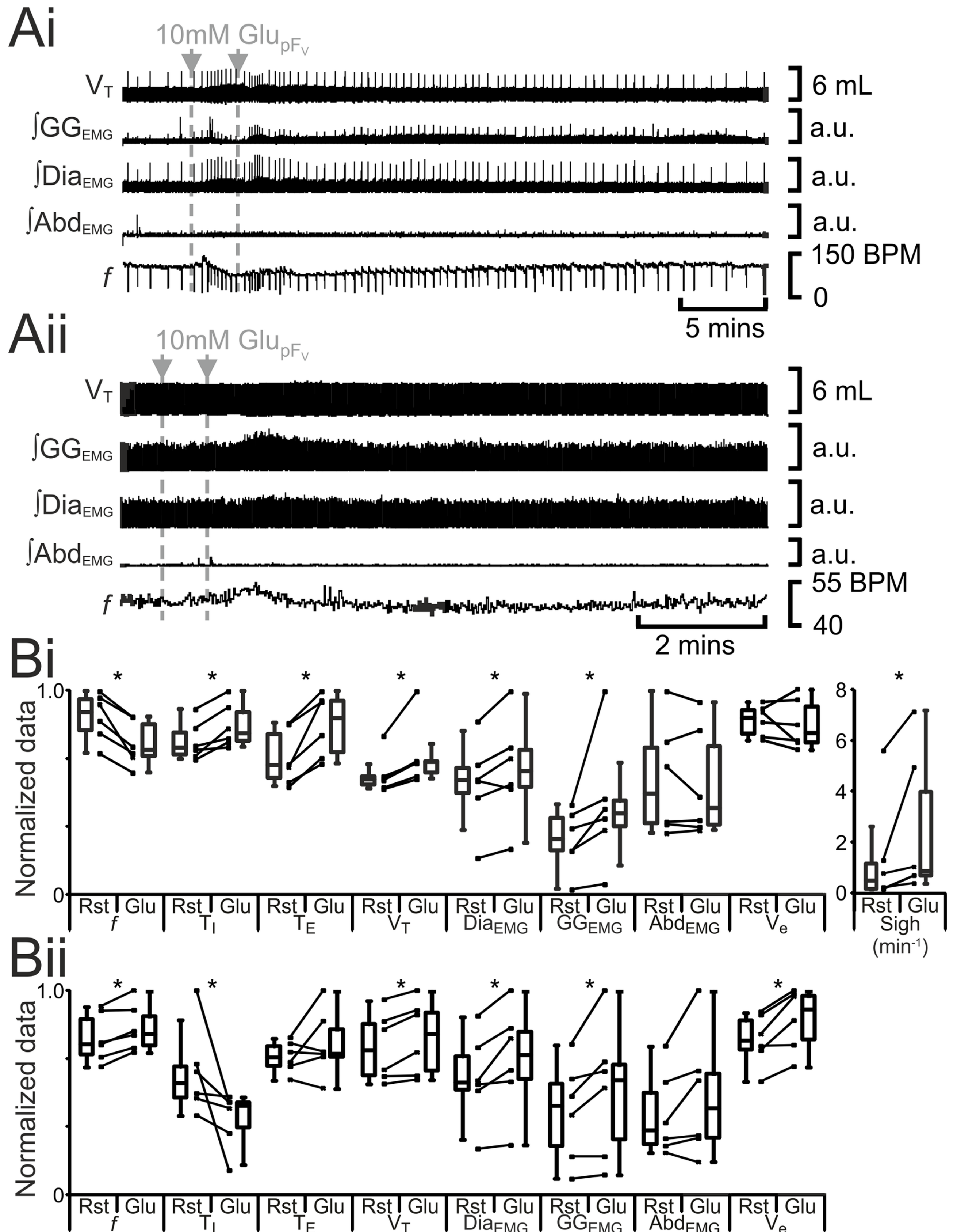
Ai
10mM Glu pFV
VT
∫GGEMG
∫DiaEMG
∫AbdEMG
f
6 mL
a.u.
a.u.
a.u.
150 BPM
0
5 mins
Aii
10mM Glu pFV
VT
∫GGEMG
∫DiaEMG
∫AbdEMG
f
6 mL
a.u.
a.u.
a.u.
55 BPM
40
2 mins
Bi
Normalized data
1.0
0
Rst Glu
f
TI
TE
VT
DiaEMG
GGEMG
AbdEMG
Ve
Sigh (min-1)
8
6
4
2
0
Bii
Normalized data
1.0
0
Rst Glu
f
TI
TE
VT
DiaEMG
GGEMG
AbdEMG
Ve

Fig 8. Glu_{pFV} alters, but does not induce, post-inspiratory activity in either abdominal muscles or in pre- and post-inspiratory activity in genioglossus muscles. A) Integrated traces from a single experiment, gray arrows indicate unilateral injections for Glu_{pFV}. Ai) Vagus intact. Aii) Vagotomized. B) Comparison between ventilation at rest (Rst) and after Glu_{pFV}. Bi) Vagus intact. Bii) Vagotomized. Lines connect data from individual experiments, box and whisker plots show combined data. Data are normalized to highest value for that parameter, i.e., *f*, T_I, T_E, V_T, GG_{EMG}, Dia_{EMG}, or Abd_{EMG} regardless of whether it belonged to control or Glu_{pFV} group. *: $p < 0.05$. Abbreviations defined in Fig 2.

https://doi.org/10.1371/journal.pone.0201485.g008

decreased *f* with a compensatory increase in V_T and inspiratory Dia_{EMG} and GG_{EMG}, and onset of expiratory bursting on GG_{EMG} and Abd_{EMG}, i.e., active expiration [8, 11]. Thus, these excitatory neurons have presumptive projections to neurons in the preBötzinger Complex (preBötC) or Bötzinger Complex (BötC) [32, 33] that inhibit inspiration during expiration, i.e., reciprocal inhibition, and to excitatory premotoneurons in the caudal ventral respiratory group (cVRG) that project to abdominal muscle motoneurons [34–36]. Given the delayed increase in V_T following the induced decrease in *f*, a direct excitatory projection from the pF_L to the preBötC appears unlikely, but rather suggests an indirect pathway related to controlling pCO_2, perhaps via the pF_V. These observations are consistent with our hypothesis that the pF_L is a conditional expiratory oscillator with neurons that are tonically inhibited at rest that can be turned on either by disinhibition and/or excitation.

Multifunctional role of the pF_V

$A+N_{pFV}$ injected into the pF_V to lower its excitability, decreased V_T and inspiratory-related muscle activity, likely via projections to the preBötC and/or the rostral ventral respiratory group (rVRG) [37]. The associated delayed increase in *f* could again be explained as intrinsic to the slower time course of chemosensory feedback to maintain pCO_2. As no change in phase durations or *f* were seen, it appears unlikely that this excitatory drive to inspiration was mediated by rhythmic preBötC neurons [38]. Rather, this observation is consistent with our hypothesis of a subpopulation of tonically active pF_V neurons that provides facilitative drive to phrenic and/or other inspiratory pump motoneurons to affect V_T, but do not contribute directly to regulating *f* or inspiratory drive to genioglossal motoneurons [11]. Instead it is more likely that the pF_V affects V_T through its projections to the rVRG [39], the premotor bulbospinal relay to the phrenic nucleus for inspiratory drive [40], as this will alter V_T without directly altering other inspiratory parameters, i.e., *f* and GG_{EMG}.

$B+S_{pFV}$ to increase pF_V excitability, increased *f*, most likely through projections to the preBötC [38, 41], presumably to the same neurons that lead to an increase in *f* following optogenetic photostimulation of the pF_V [42, 43]. $B+S_{pFV}$ also increased inspiratory-related GG_{EMG}, likely through pF_V projections to the parahypoglossal region (pXII) [39], which appears to be the premotor relay for inspiratory drive to the XII nucleus [44]. Though $B+S_{pFV}$ attenuated Dia_{EMG} and V_T, this appeared secondary to the reduction in *f* and thus was most likely due to chemosensory feedback to control pCO_2. This further supports our hypothesis of a subpopulation of tonically suppressed pF_V neurons that provide facilitative drive to modulate *f*, but does not contribute directly to V_T.

Unlike $B+S_{pFV}$, $AMPA_{pFV}$ potentiated V_T and Dia_{EMG} activity, most likely through excitation of the neurons that were attenuated by $A+N_{pFV}$ and project to the rVRG. $AMPA_{pFV}$ also increased *f* and inspiratory-related GG_{EMG} most likely through excitation of neurons that project to the preBötC and parahypoglossal region that were activated following $B+S_{pFV}$. As $B+S_{pFV}$ and $AMPA_{pFV}$ each led to different patterns of breathing with neither similar to the effects of activating the pF_L, we suggest that there are at least two relevant pF_V subpopulations, one expressing inhibitory receptors and one that does not, and that both of these subgroups are distinct from the pF_L.

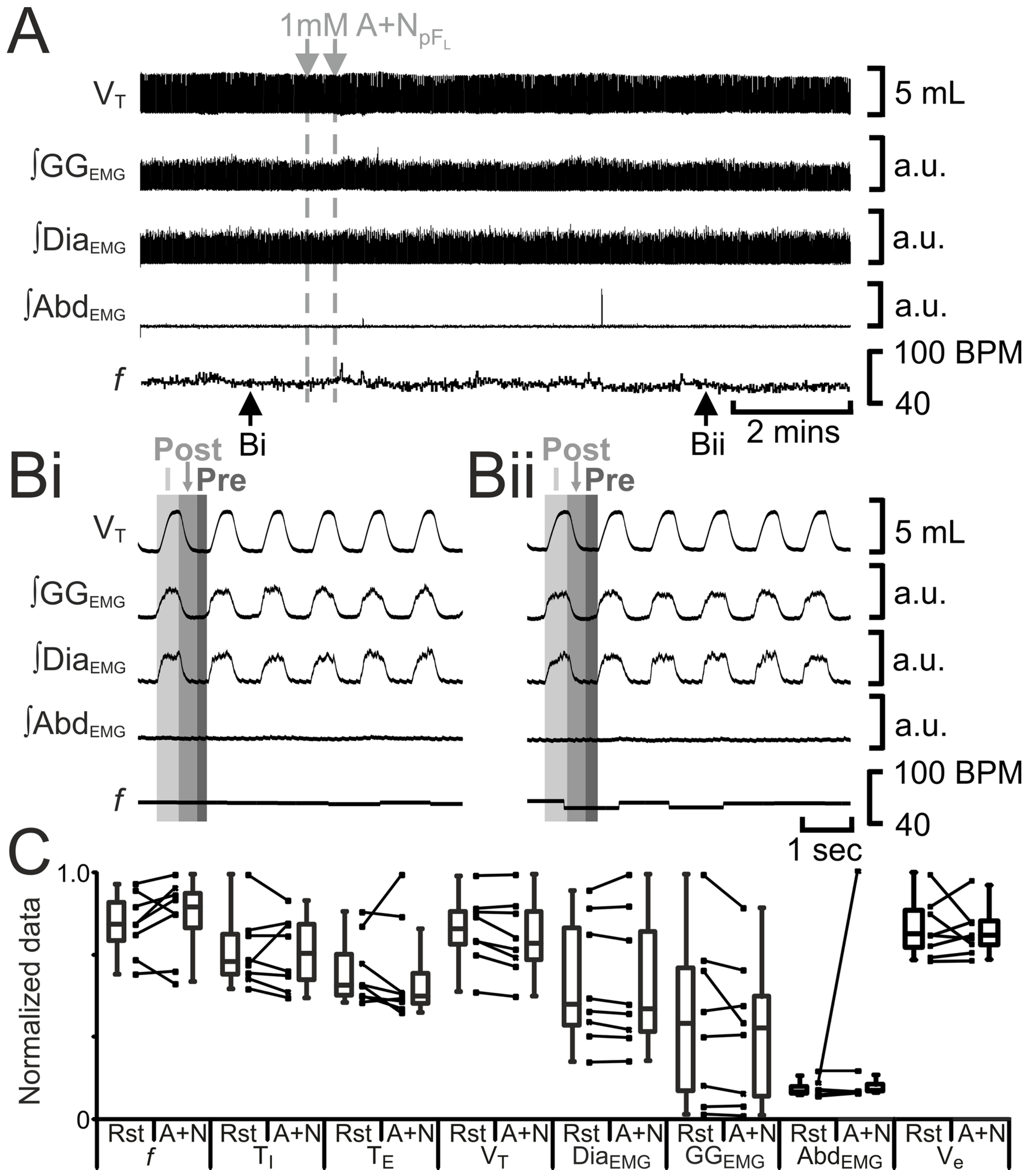
A
1mM A+N$_{pF_L}$
V_T
∫GG$_{EMG}$
∫Dia$_{EMG}$
∫Abd$_{EMG}$
f
5 mL
a.u.
a.u.
a.u.
100 BPM
40
2 mins
Bi
Bii
Bi
Post
I
Pre
Bii
Post
I
Pre
1 sec
C
Normalized data
1.0
0
Rst
A+N
f
T_I
T_E
V_T
Dia$_{EMG}$
GG$_{EMG}$
Abd$_{EMG}$
V_e

Fig 9. A+N_{pFL} does not affect breathing. A) Integrated traces from a single experiment. Black arrows at bottom indicate epochs in expanded traces (Bi and Bii), gray arrows at top indicate unilateral injections for A+N_{pFL}. Bi) Rest. Bii) Following A+N_{pFL}. Grey vertical boxes demark phases of each breath: inspiration (I; light gray), post-inspiration (Post: medium grey), and pre-inspiration (Pre: Dark gray). C) Comparison between ventilation at rest (Rst) and after A+N_{pFL} injection. Lines connect data from individual experiments, box and whisker plots show combined data. Data are normalized to highest value for each parameter, i.e., *f*, T_I, T_E, V_T, GG_{EMG}, Dia_{EMG}, or Abd_{EMG} regardless of whether it belonged to control or A+N_{pFL} group. Abbreviations defined in Fig 2.

https://doi.org/10.1371/journal.pone.0201485.g009

Similar to stimulation of pF_V neurons in awake behaving vagus intact rats [23] and in vagotomized urethane anesthetized cats [22], disinhibition with B+S_{pFV} elicited sighs in vagotomized rats (Fig 3Bii#), as did excitation with Glu_{pFV} in vagus-intact rats (Fig 8A). In vagotomized rats the amplitude of normal breaths is considerably larger than vagus-intact rats, with the consequence that sighs are masked. Accordingly, when V_T was low, i.e., in vagus-intact rats or following a reduction in amplitude caused by B+S_{pFV} in vagotomized rats, sustained increases in sigh activity could be seen. This confirms our recent study showing a cluster of neurons in the pF_V that release bombesin-like neuropeptides that affect sighing through the activation of cognate receptors in the preBötC [16].

Hyperpolarizing pF_V neurons during hypercapnia and hypoxia affects the amplitude of Abd_{EMG} and GG_{EMG}, but not V_T or *f* [11], likely through direct projections to the cVRG [15] and parahypoglossal region [39]. Interestingly, B+S_{pFV} induced high amplitude post-inspiratory activity on both GG_{EMG} and Abd_{EMG}, likely through the same projections, supporting our previous finding that the pF_V provides excitatory drive to expiratory premotor nuclei independent of its projections to the preBötC [11]. Interestingly, no perturbation of pF_V excitability induced active expiration, while hyperpolarization of the pF_V reduces active expiration during chemosensory stimulation [11, 13]. We conclude that the pF_V provides can modulate expiratory activity generated elsewhere, but cannot itself induce active expiration.

Interestingly, most manipulations which changed either *f* or V_T led to compensatory changes, presumably to regulate V_E to control pCO_2 to within the normal range. For example, reducing excitation in the pF_V reduced activity of neurons that influence diaphragmatic (pre) motoneurons, which are constitutively active at rest. Thus, this manipulation reduced V_T, but had no effect on *f* as the pF_V neurons that influence *f* were supressed at rest and therefore their activity could not be affected by A+N; this allows for other brain regions to affect preBötC rhythmogenic neurons to increase *f* to compensate for the reduction in V_T. Only one manipulation, glutamatergic activation of the pF_V (with either AMPA or Glu) changed V_E. We believe that this is because glutamatergic activation of the pF_V RTN leads to activation of the tonically supressed neurons that activate preBötC rhythmogenic neurons; furthermore this manipulation also excites the neurons that are active at rest that influence diaphragmatic (pre)motoneurons, consequently altering both *f* and V_T simultaneously.

Summary

We propose that there are at least 6 subpopulations of parafacial neurons (Fig 11). The pF_L is a conditional expiratory oscillator, with a functionally homogeneous population of neurons that drive active expiration (Fig 11). By contrast, the pF_V provides a critical generic facilitatory drive to breathe, and consists of at least 4 functionally distinct subpopulations of neurons: i) a tonically active subpopulation that drives V_T via the diaphragm; ii) one subpopulation of tonically suppressed neurons that modulate *f*; and; iii) a second subpopulation of tonically suppressed neurons that provide drive to abdominal and genioglossus expiratory motor pools, iv) a subpopulation of bombesin-peptide, i.e., NMB, neurons of the hypothesized peptidergic sigh circuit [16]. In addition, there is a 6th subpopulation bombesin-peptide, i.e., GRP, neurons in the dorsocaudal parafacial (pF_{DC}) that also can modulate basal sigh rate [16].

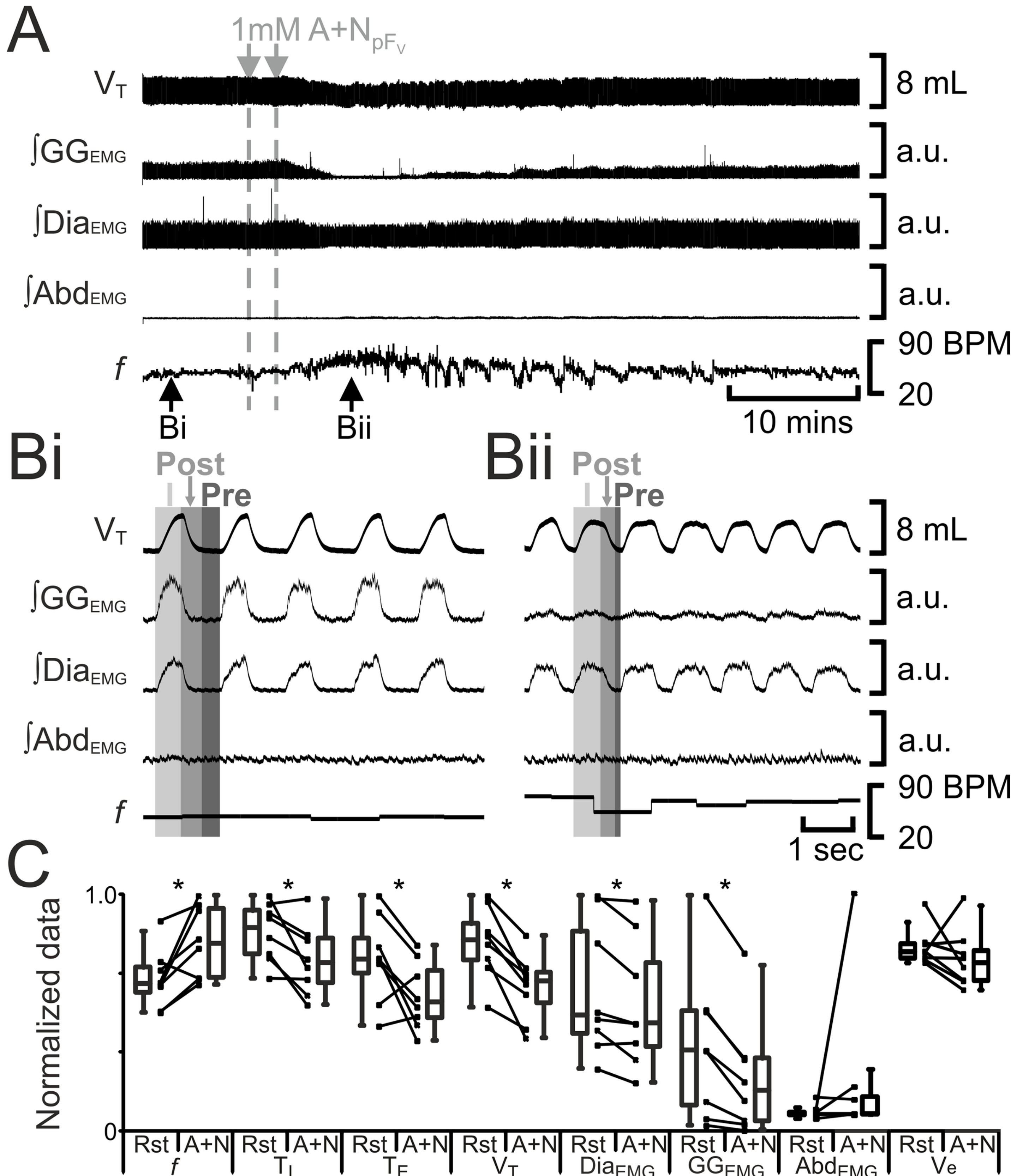

Fig 10. A+N$_{pFV}$ decreases V$_T$, and reduces output of inspiratory muscles. A) Integrated traces from a single experiment. Black arrows at bottom indicate epochs in expanded traces (Bi and Bii), gray arrows at top indicate unilateral injections for A+N$_{pFV}$. Bi) Rest. Bii) Following A+N$_{pFV}$. Grey vertical boxes demark phases of each

breath: inspiration (I; light gray), post-inspiration (Post: medium grey), and pre-inspiration (Pre: Dark gray). C) Comparison between ventilation at rest (Rst) and after A+N$_{pFV}$ injection. Lines connect data from individual experiments, box and whisker plots show combined data. Data are normalized to highest value for each parameter, i.e., *f*, T_I, T_E, V_T, GG_{EMG}, Dia_{EMG}, or Abd_{EMG} regardless of whether it belonged to control or A+N$_{pFV}$ group. *: $p < 0.05$. Abbreviations defined in Fig 2.

https://doi.org/10.1371/journal.pone.0201485.g010

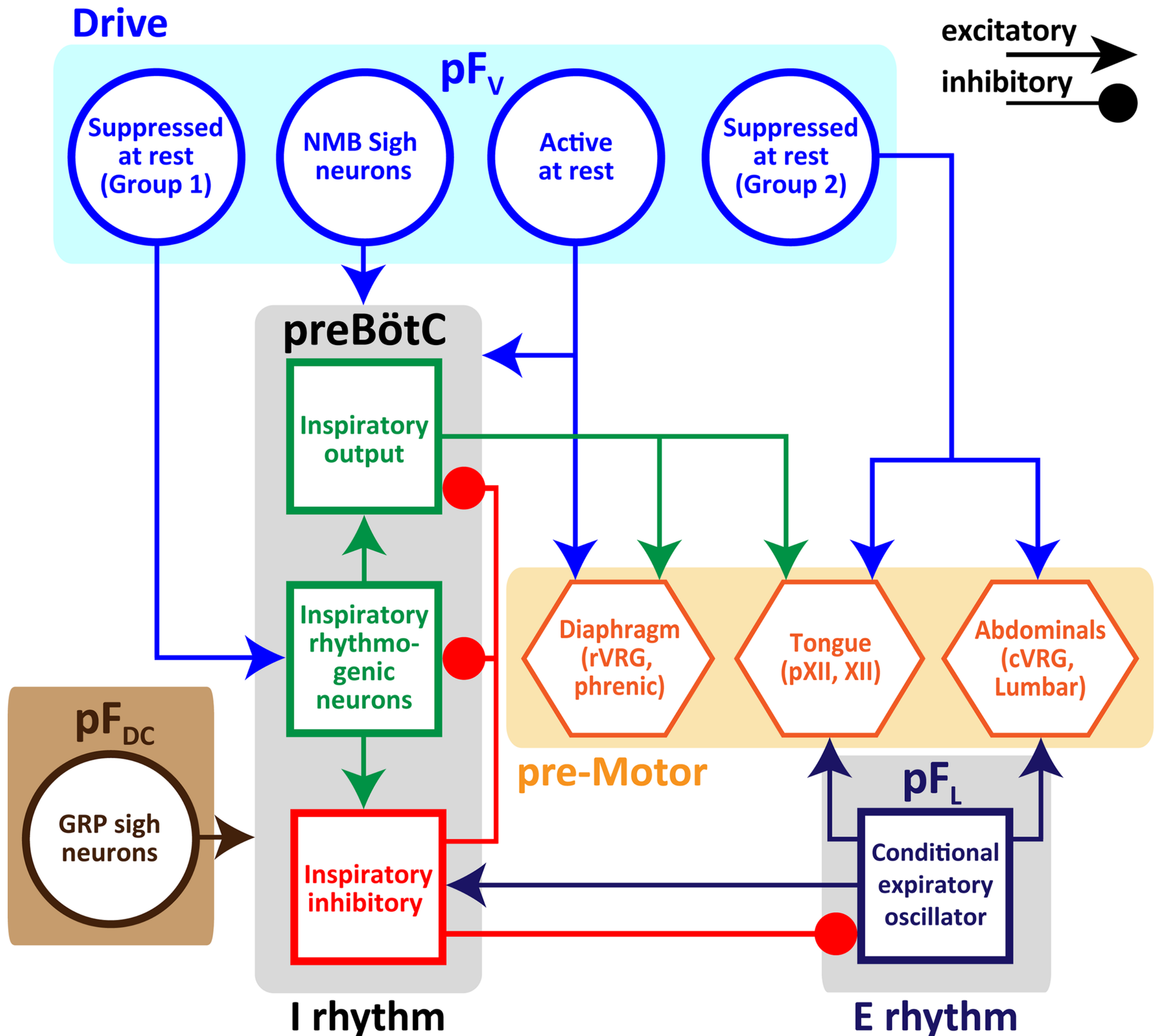

Fig 11. Schematic of minimal bCPG, which consists of 4 essential components. 1) preBötzinger Complex (preBötC) drives inspiration by exciting inspiratory premotor neuronal populations projecting to inspiratory muscles, e.g., diaphragm and tongue, and inhibits pF$_L$; 2) parafacial Dorsocaudal (pF$_{DC}$) contains GRP positive neurons contributing to basal sigh rhythm. 3) pF$_L$ drives active expiration by exciting expiratory premotor neuronal populations projecting to expiratory muscles, e.g., abdominals and tongue, and excites neurons that inhibit preBötC, either in preBötC or in BötC (not shown); 4) pF$_V$ contains neurons and glia that contribute to CO_2/pH regulation and integrates sensory afferents affecting breathing, including basal sigh rate, via excitatory connections to preBötC and breathing premotor and motor neurons. pF$_V$ contains 4 subpopulations: i) tonically active neurons that modulate V_T and diaphragm bursting at rest; ii) tonically suppressed neurons that modulate *f*; iii) NMB positive neurons that affect basal sigh rate, and; iv) tonically suppressed neurons that provide rhythmic drive to abdominal and genioglossus expiratory motor pools producing active expiration.

https://doi.org/10.1371/journal.pone.0201485.g011

Author Contributions

Conceptualization: Robert T. R. Huckstepp, Jack L. Feldman.

Data curation: Robert T. R. Huckstepp, Kathryn P. Cardoza, Lauren E. Henderson.

Formal analysis: Robert T. R. Huckstepp.

Funding acquisition: Jack L. Feldman.

Methodology: Robert T. R. Huckstepp, Jack L. Feldman.

Writing – original draft: Robert T. R. Huckstepp, Jack L. Feldman.

Writing – review & editing: Robert T. R. Huckstepp, Kathryn P. Cardoza, Lauren E. Henderson, Jack L. Feldman.

References

1. Champagnat J, Fortin G. Primordial respiratory-like rhythm generation in the vertebrate embryo. Trends Neurosci. 1997; 20(3):119–24. http://dx.doi.org/10.1016/S0166-2236(96)10078-3. PMID: 9061866
2. Champagnat J, Thoby-Brisson M, Fortin G. Chapter 3—Genetic factors determining the functional organization of neural circuits controlling rhythmic movements: the murine embryonic parafacial rhythm generator. Prog Brain Res. 2010; 187:39–46. https://doi.org/10.1016/B978-0-444-53613-6.00003-4 PMID: 21111199
3. Mulkey DK, Stornetta RL, Weston MC, Simmons JR, Parker A, Bayliss DA, et al. Respiratory control by ventral surface chemoreceptor neurons in rats. Nat Neurosci. 2004; 7(12):1360–9. https://doi.org/10.1038/nn1357 PMID: 15558061
4. Ramanantsoa N, Hirsch MR, Thoby-Brisson M, Dubreuil V, Bouvier J, Ruffault PL, et al. Breathing without CO_2 chemosensitivity in conditional Phox2b mutants. J Neurosci. 2011; 31(36):12880–8. Epub 2011/09/09. https://doi.org/10.1523/JNEUROSCI.1721-11.2011 PMID: 21900566.
5. Nattie EE, Li A. Substance P-saporin lesions of neurons with NK1 receptors in one chemosensitive site in rats decreases ventillation and chemosensitivity. J Physiol. 2002; 544(2):603–16.
6. Onimaru H, Ikeda K, Kawakami K. CO2-sensitive preinspiratory neurons of the parafacial respiratory group express Phox2b in the neonatal rat. J Neurosci. 2008; 28(48):12845–50. https://doi.org/10.1523/JNEUROSCI.3625-08.2008 PMID: 19036978
7. Onimaru H, Homma I. A novel functional neuron group for respiratory rhythm generation in the ventral medulla. J Neurosci. 2003; 23(4):1478–86. PMID: 12598636
8. Pagliardini S, Janczewski WA, Tan W, Dickson CT, Deisseroth K, Feldman JL. Active expiration induced by excitation of ventral medulla in adult anesthetized rats. J Neurosci. 2011; 31(8):2895–905. https://doi.org/10.1523/JNEUROSCI.5338-10.2011 PMID: 21414911
9. Oku Y, Masumiya H, Okada Y. Postnatal developmental changes in activation profiles of the respiratory neuronal network in the rat ventral medulla. J Physiol. 2007; 585(1):175–86.
10. Mellen NM, Janczewski WA, Bocchiaro CM, Feldman JL. Opioid-induced quantal slowing reveals dual networks for respiratory rhythm generation. Neuron. 2003; 37(5):821–6. PMID: 12628172.
11. Huckstepp RTR, Cardoza KP, Henderson LE, Feldman JL. Role of parafacial nuclei in control of breathing in adult rats. J Neurosci. 2015; 35:1052–67. https://doi.org/10.1523/JNEUROSCI.2953-14.2015 PMID: 25609622
12. Janczewski WA, Feldman JL. Distinct rhythm generators for inspiration and expiration in the juvenile rat. J Physiol. 2006; 570(2):407–20.
13. Marina N, Abdala AP, Trapp S, Li A, Nattie EE, Hewinson J, et al. Essential role of Phox2b-expressing ventrolateral brainstem neurons in the chemosensory control of inspiration and expiration. J Neurosci. 2010; 30(37):12466–73. Epub 2010/09/17. https://doi.org/10.1523/JNEUROSCI.3141-10.2010 PMID: 20844141; PubMed Central PMCID: PMC3026590.
14. Abbott SBG, Stornetta RL, Coates MB, Guyenet PG. Phox2b-expressing neurons of the parafacial region regulate breathing rate, inspiration, and expiration in conscious rats. J Neurosci. 2011; 31(45):16410–22. https://doi.org/10.1523/JNEUROSCI.3280-11.2011 PMID: 22072691
15. Silva JN, Tanabe FM, Moreira TS, Takakura AC. Neuroanatomical and physiological evidence that the retrotrapezoid nucleus/parafacial region regulates expiration in adult rats. Respir Physiol Neurobiol. 2016; 227:9–22. https://doi.org/10.1016/j.resp.2016.02.005 PMID: 26900003

16. Li P, Janczewski WA, Yackle K, Kam K, Pagliardini S, Krasnow MA, et al. The peptidergic control circuit for sighing. Nature. 2016; 530(7590):293–7. https://doi.org/10.1038/nature16964 http://www.nature.com/nature/journal/v530/n7590/abs/nature16964.html#supplementary-information. PMID: 26855425

17. Swanson LW, Sawchenko PE. Paraventricular Nucleus:A Site for the Integration of Neuroendocrine and Autonomic Mechanisms. Neuroendocrinology. 1980; 31(6):410–7. https://doi.org/10.1159/000123111 PMID: 6109264

18. Loewy AD, Burton H. Nuclei of the solitary tract: Efferent projections to the lower brain stem and spinal cord of the cat. J Comp Neurol. 1978; 181(2):421–49. https://doi.org/10.1002/cne.901810211 PMID: 690272

19. Bandler R, Shipley MT. Columnar organization in the midbrain periaqueductal gray: modules for emotional expression? Trends Neurosci. 1994; 17(9):379–89. https://doi.org/10.1016/0166-2236(94)90047-7. PMID: 7817403

20. Faul F, Erdfelder E, Lang A-G, Buchner A. G*Power 3: A flexible statistical power analysis program for the social, behavioral, and biomedical sciences. Behavior Research Methods. 2007; 39(2):175–91. https://doi.org/10.3758/BF03193146 PMID: 17695343

21. Nattie EE, Shi J, Li A. Bicuculline dialysis in the retrotrapezoid nucleus (RTN) region stimulates breathing in the awake rat. Respir Physiol 2001; 124(3):179–93. http://dx.doi.org/10.1016/S0034-5687(00)00212-7. PMID: 11173073

22. Nattie EE, Li A. Retrotrapezoid nucleus glutamate injections: long-term stimulation of phrenic activity. J Appl Physiol. 1994; 76(2):760–72. https://doi.org/10.1152/jappl.1994.76.2.760 PMID: 7909799

23. Abbott SBG, Coates MB, Stornetta RL, Guyenet PG. Optogenetic stimulation of C1 and retrotrapezoid nucleus neurons causes sleep state–dependent cardiorespiratory stimulation and arousal in rats. Hypertension. 2013; 61(4):835–41. https://doi.org/10.1161/HYPERTENSIONAHA.111.00860 PMID: 23438930

24. de Britto AA, Moraes DJA. Non-chemosensitive parafacial neurons simultaneously regulate active expiration and airway patency under hypercapnia in rats. J Physiol. 2017; 595(6):2043–64. https://doi.org/10.1113/JP273335 PMID: 28004411

25. Nattie EE. Multiple sites for central chemoreception: their role in response sensitivity and in sleep and wakefullness. Resp Physiol. 2000; 122:223–35.

26. Mulkey DK, Rosin DL, West G, Takakura AC, Moreira TS, Bayliss DA, et al. Serotonergic neurons activate chemosensitive retrotrapezoid nucleus neurons by a pH-independent mechanism. J Neurosci. 2007; 27(51):14128–38. https://doi.org/10.1523/JNEUROSCI.4167-07.2007 PMID: 18094252

27. Li A, Zhou S, Nattie EE. Simultaneous inhibition of caudal medullary raphe and retrotrapezoid nucleus decreases breathing and the CO_2 response in conscious rats. J Physiol. 2006; 577(1):307–18.

28. Nattie EE, Li A. CO_2 dialysis in nucleus tractus solitarius region of rat increases ventilation in sleep and wakefulness. J Appl Physiol. 2002; 92:2119–30. https://doi.org/10.1152/japplphysiol.01128.2001 PMID: 11960965

29. Moreira TS, Takakura AC, Colombari E, Guyenet PG. Activation of 5-hydroxytryptamine type 3 receptor-expressing C-fiber vagal afferents inhibits retrotrapezoid nucleus chemoreceptors in rats. J Neurophysiol. 2007; 98(6):3627–37. https://doi.org/10.1152/jn.00675.2007 PMID: 17928558

30. Janczewski WA, Feldman JL. Novel data supporting the two respiratory rhythm oscillator hypothesis. focus on "respiration-related rhythmic activity in the rostral medulla of newborn rats". J Neurophysiol. 2006; 96:1–2. https://doi.org/10.1152/jn.00246.2006 PMID: 16554514

31. Huckstepp RTR, Henderson LE, Cardoza KP, Feldman JL. Interactions between respiratory oscillators in adult rats. eLife. 2016; 5:e14203. https://doi.org/10.7554/eLife.14203 PMID: 27300271

32. Morgado-Valle C, Baca SM, Feldman JL. Glycinergic pacemaker neurons in preBötzinger Complex of neonatal mouse. J Neurosci. 2010; 30(10):3634–9. https://doi.org/10.1523/JNEUROSCI.3040-09.2010 PMID: 20219997

33. Schreihofer AM, Stornetta RL, Guyenet PG. Evidence for glycinergic respiratory neurons: Bötzinger neurons express mRNA for glycinergic transporter 2. J Comp Neurol. 1999; 407(4):583–97. https://doi.org/10.1002/(SICI)1096-9861(19990517)407:4<583::AID-CNE8>3.0.CO;2-E PMID: 10235646

34. Iscoe S. Control of abdominal muscles. Prog Neurobiol. 1998; 56(4):433–506. PMID: 9775401

35. Cinelli E, Bongianni F, Pantaleo T, Mutolo D. Modulation of the cough reflex by $GABA_A$ receptors in the caudal ventral respiratory group of the rabbit. Front Physiol. 2012; 3:403. https://doi.org/10.3389/fphys.2012.00403 PMID: 23087651

36. Janczewski WA, Onimaru H, Homma I, Feldman JL. Opioid-resistant respiratory pathway from the pre-inspiratory neurones to abdominal muscles: in vivo and in vitro study in the newborn rat. J Physiol. 2002; 545(3):1017–26. https://doi.org/10.1113/jphysiol.2002.023408 PMID: 12482904

37. Núñez-Abades PA, Morillo AM, Pásaro R. Brainstem connections of the rat ventral respiratory subgroups: afferent projections. J Auton Nerv Syst. 1993; 42(2):99–118. PMID: 8383713

38. Cui Y, Kam K, Sherman D, Janczewski WA, Zheng Y, Feldman JL. Defining preBötzinger Complex rhythm- and pattern-generating neural microcircuits *in vivo*. Neuron. 2016; 91(3):602–14. https://doi.org/10.1016/j.neuron.2016.07.003 PMID: 27497222

39. Rosin DL, Chang DA, Guyenet PG. Afferent and efferent connections of the rat retrotrapezoid nucleus. J Comp Neurol. 2006; 499(1):64–89. Epub 2006/09/08. https://doi.org/10.1002/cne.21105 PMID: 16958085.

40. Portillo F, Nunez-Abades A. Distribution of bulbospinal neurones supplying bilateral innervation to the phrenic nucleus in the rat. Brain Res. 1992; 583:349–55. PMID: 1380401

41. Smith JC, Morrison DE, Ellenberger HH, Otto MR, Feldman JL. Brainstem projections to the major respiratory neuron populations in the medulla of the cat. J Comp Neurol. 1989; 281(1):69–96. https://doi.org/10.1002/cne.902810107 PMID: 2466879.

42. Abbott SBG, Stornetta RL, Socolovsky CS, West GH, Guyenet PG. Photostimulation of channelrhodopsin-2 expressing ventrolateral medullary neurons increases sympathetic nerve activity and blood pressure in rats. J Physiol. 2009; 587(23):5613–31. https://doi.org/10.1113/jphysiol.2009.177535 PMID: 19822543

43. Burke PGR, Kanbar R, Viar KE, Stornetta RL, Guyenet PG. Selective optogenetic stimulation of the retrotrapezoid nucleus in sleeping rats activates breathing without changing blood pressure or causing arousal or sighs. J Appl Physiol. 2015; 118(12):1491–501. https://doi.org/10.1152/japplphysiol.00164.2015 PubMed PMID: PMC4469924. PMID: 25858492

44. Chamberlin NL, Eikermann M, Fassbender P, White DP, Malhotra A. Genioglossus premotoneurons and the negative pressure reflex in rats. J Physiol. 2007; 579(2):515–26. https://doi.org/10.1113/jphysiol.2006.121889 PMID: 17185342